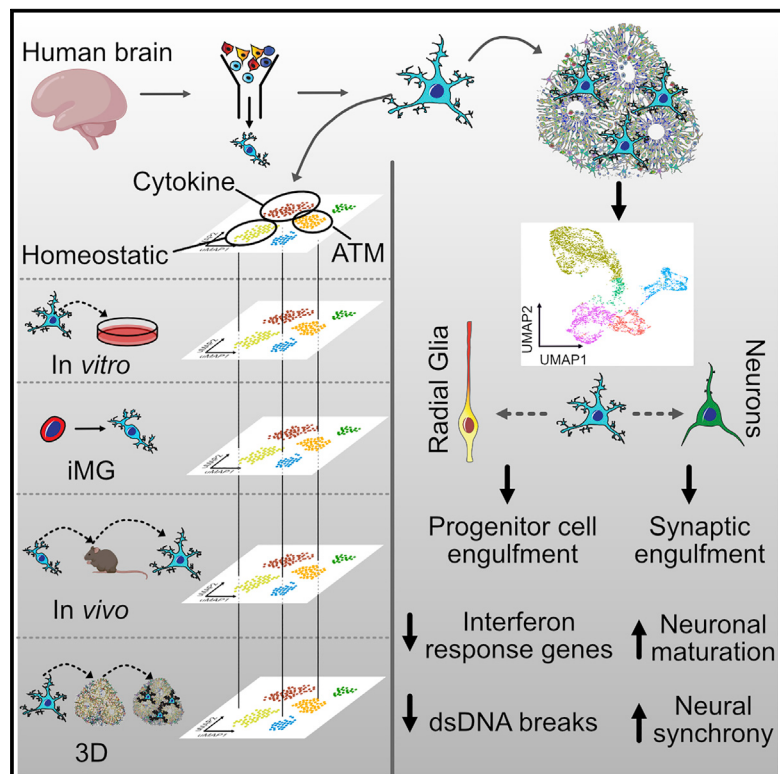


Human microglia states are conserved across experimental models and regulate neural stem cell responses in chimeric organoids

Graphical abstract



Authors

Galina Popova, Sarah S. Soliman,
Chang N. Kim, ...,
Richard R. Ransohoff, Xianhua Piao,
Tomasz J. Nowakowski

Correspondence

tomasz.nowakowski@ucsf.edu

In brief

Our “microglia report card” reveals that human microglia selectively regulate different biological gene cluster modules in an environment-dependent fashion. The presence of microglia in brain organoids protects against double-stranded DNA breaks and attenuates the gene response on the interferon signaling pathway. Additionally, microglia accelerate neural network synchronization in organoids.

Highlights

- Microglia culture models differentially attenuate and preserve gene signatures
- Brain organoid microenvironment preserves microglial homeostatic state
- Genes in the interferon response pathway are attenuated in the presence of microglia
- Microglia decrease double-stranded DNA breaks and cell stress in radial glia



Resource

Human microglia states are conserved across experimental models and regulate neural stem cell responses in chimeric organoids

Galina Popova,^{1,2,3} Sarah S. Soliman,^{1,2,3} Chang N. Kim,^{1,2,3} Matthew G. Keefe,^{1,2,3} Kelsey M. Hennick,^{1,2,3} Samhita Jain,⁴ Tao Li,^{3,5} Dario Tejera,^{3,5} David Shin,^{1,2,3} Bryant B. Chhun,⁶ Christopher S. McGinnis,⁷ Matthew Speir,⁸ Zev J. Gartner,^{6,7,9,10} Shalin B. Mehta,⁶ Maximilian Haeussler,⁸ Keith B. Hengen,¹¹ Richard R. Ransohoff,¹² Xianhua Piao,^{3,4,5,13} and Tomasz J. Nowakowski^{1,2,3,5,6,14,*}

¹Department of Anatomy, University of California, San Francisco, San Francisco, CA, USA

²Department of Psychiatry, University of California, San Francisco, San Francisco, CA, USA

³Eli and Edythe Broad Center for Regeneration Medicine and Stem Cell Research, University of California, San Francisco, San Francisco, CA, USA

⁴Division of Neonatology, Department of Pediatrics, University of California, San Francisco, San Francisco, CA, USA

⁵Weill Institute for Neurosciences, University of California, San Francisco, San Francisco, CA, USA

⁶Chan Zuckerberg Biohub, San Francisco, CA, USA

⁷Department of Pharmaceutical Chemistry, University of California, San Francisco, San Francisco, CA USA

⁸Genomics Institute, University of California, Santa Cruz, Santa Cruz, CA, USA

⁹Center for Cellular Construction, University of California, San Francisco, San Francisco, CA, USA

¹⁰Helen Diller Family Comprehensive Cancer Center, University of California, San Francisco, San Francisco, CA, USA

¹¹Department of Biology, Washington University in St. Louis, St. Louis, MO, USA

¹²Department of Cell Biology, Harvard Medical School, Boston, MA, USA

¹³Newborn Brain Research Institute, University of California, San Francisco, San Francisco, CA, USA

¹⁴Lead contact

*Correspondence: tomasz.nowakowski@ucsf.edu

<https://doi.org/10.1016/j.stem.2021.08.015>

SUMMARY

Microglia are resident macrophages in the brain that emerge in early development and respond to the local environment by altering their molecular and phenotypic states. Fundamental questions about microglia diversity and function during development remain unanswered because we lack experimental strategies to interrogate their interactions with other cell types and responses to perturbations *ex vivo*. We compared human microglia states across culture models, including cultured primary and pluripotent stem cell-derived microglia. We developed a “report card” of gene expression signatures across these distinct models to facilitate characterization of their responses across experimental models, perturbations, and disease conditions. Xenotransplantation of human microglia into cerebral organoids allowed us to characterize key transcriptional programs of developing microglia *in vitro* and reveal that microglia induce transcriptional changes in neural stem cells and decrease interferon signaling response genes. Microglia additionally accelerate the emergence of synchronized oscillatory network activity in brain organoids by modulating synaptic density.

INTRODUCTION

Microglia are resident macrophages of the brain and have been shown to respond to many viral pathogens to protect neurons and glia from pathogen-induced damage (Garden 2002; Retallack et al., 2016; Bortolotti et al., 2019). Mutations in microglia-related genes have been implicated in a wide range of neurological (Rademakers et al., 2011; Oosterhof et al., 2019), neuropsychiatric (Needleman and McAllister, 2012; Sekar et al., 2016), and neurodegenerative diseases (Krasemann et al., 2017). Moreover, microglia have been shown to adopt dis-

ease-associated transcriptional states in a wide variety of disease environments (Keren-Shaul et al., 2017; Li et al., 2019; Matsuda et al., 2019). Finally, microglia transcriptomes have been shown to vary substantially across species (Geirsdottir et al., 2019), suggesting that, to dissect the contributions of microglia to neurodevelopmental and disease processes in the human brain, human cell-based experimental models may be required. However, it is unclear which models can best recapitulate the molecular architecture of human microglia subpopulations because microglia are known to undergo substantial changes in gene expression upon isolation from the brain parenchyma



as well as across culture models (Gosselin et al., 2017). A comprehensive molecular map of microglia diversity across experimental models would enable data-driven decisions regarding the most relevant experimental systems.

By harnessing single-cell transcriptomics, we sought to create a comprehensive “report card” for human microglia during development. We found that a three-dimensional neural tissue environment presents the strongest transcriptomic correlations of microglia to their *in vivo* counterparts. In particular, xenotransplantation of microglia into brain organoids that are largely devoid of myeloid lineage cells allows systematic comparison of neurodevelopmental processes in the presence or absence of microglia. Interestingly, we found widespread expression of genes involved in the type I interferon response in organoid radial glia that becomes attenuated in the presence of microglia. In contrast, neurons appear to be transcriptionally invariant to microglia transplantation but instead undergo synaptic remodeling and accelerated maturation of network properties. Our work highlights the molecular plasticity of human microglia across culture models, underscores the potential shortcomings of microglia derived from pluripotent stem cells in recapitulating *in vivo* signatures, and reveals transcriptional responses of developing human neural tissue to the presence of microglia.

RESULTS

A microglia “report card” across culture models

Efficient culture models of human microglia are required to advance our understanding of normal brain development and neuroimmune interactions in disease states. Unfortunately, transcriptomic and morphological changes in cultured microglia (Gosselin et al., 2017) are a significant challenge for human microglia studies. To characterize which microglia subtypes are preserved and how they change across different models, we generated new single-cell RNA sequencing data from two *in vitro* models and combined them with a previously published humanized mouse model engrafted with human induced pluripotent stem cell (iPSC)-derived microglia (iMGs) (Svoboda et al., 2019). To avoid microglia exposure to peripheral blood-derived secreted factors that have been shown to induce quick changes in gene expression in cultured microglia (Gosselin et al., 2017), we used a serum-free culture medium that has been shown to promote microglia survival *in vitro* (Bohlen et al., 2017; Montilla et al., 2020). We purified primary microglia using magnetic-activated cell sorting (MACS) with beads binding CD11b, and cultured the cells as a monolayer culture under serum-free conditions supplemented with interleukin-34 (IL-34), transforming growth factor β 2 (TGF- β 2), and cholesterol to provide the trophic conditions necessary for microglia survival (Bohlen et al., 2017; Figures 1A and 1D; STAR Methods). For the duration of the culture, microglia remained ramified and motile (Video S1). After 8 days in culture, microglia expressed Iba1, a broad macrophage marker, and P2RY12, a microglia-specific marker that has been reported previously to be downregulated under *ex vivo* conditions (Gosselin et al., 2017; Figure S1A). Next we explored conservation of microglia signatures across common experimental models, including microglia that were induced from pluripotent stem cells using a recently established protocol (Abud et al., 2017; Figures 1B and 1E; Figure S1; STAR Methods). We also

analyzed published data from induced microglia that had been transplanted into *in vivo* mouse brains (Svoboda et al., 2019; Figures 1C and 1F; Figure S1). To perform an unbiased comparison of microglia states in the native brain environment and in culture and to determine whether microglia heterogeneity is preserved *in vitro*, we compared these combined single-cell RNA sequencing (scRNA-seq) datasets with data from primary human microglia from the BRAIN Initiative Cell Consensus Network (BICCN) that were combined with scRNA-seq data from the developing human hippocampus (Zhong et al., 2020). For the primary clustered microglia cells that were *in silico* purified from samples ranging from gestational week 16 (GW16)–GW27, we excluded clusters that were enriched for gene markers of B cells (*CD79B*, *IGHM*, and *IGKC*), natural killer cells (*NKG7*, *PRF1*, and *KLRB1*), and dividing cells (Figure S2A). After iteratively clustering the resulting microglia, we identified five molecularly unique clusters of microglia, all of which expressed high levels of the pan-macrophage marker *Alf1* (Figures S2B and S2C, Figure S3). Cluster 1 was characterized by high expression of *LGALS1*, *LGALS3*, *APOC1*, *FTL*, and *SPP1*, recapitulating a microglia subtype that has been described previously (Hammond et al., 2019; Li et al., 2019). In accordance with these reports, we call this microglia cluster axon tract-associated microglia (ATMs). Cluster 2 expressed high levels of chemokines and cytokines (*CCL3*, *CCL4*, *CXCL8*, and *IL1B*), and we call it cytokine-associated microglia. Cluster 3 had a gene signature consisting of heat shock proteins and immediate-early genes (*JUN*, *RHOB*, *HSPA1A*, and *DNAJB1*) that has been shown previously to be induced by enzymatic digestion of primary brain tissue (Marsh et al., 2020); therefore, we call it ex-vivo-activated microglia. Cluster 4 had higher expression of genes associated with mature homeostatic microglia (*CX3CR1*, *P2RY12*, *P2RY13*, and *VSIR*); therefore we call it homeostatic microglia. Finally, a small cluster 5 was defined by a gene signature (*F13A1*, *MRC1*, and *LYVE1*) consistent with perivascular macrophages (PVMs) (Zeisel et al., 2015). We additionally performed sex-related differentially expressed gene analysis among microglia from the homeostatic and ATM clusters (Table S1; Figure S2J).

To facilitate comparison of different microglia subtypes across the models, we created a score for each transcriptionally defined microglia subtype based on an eigengene for the top 15 differentially expressed cluster markers (Figure S3) in addition to a dividing cell signature and projected these scores on the individual scRNA-seq clusters for each condition (Figures 1G–1I). In accordance with a previous report (Gosselin et al., 2017), primary microglia cultured *in vitro* had lower expression levels for the homeostatic signature (Figure 1G). Importantly, certain microglia subtypes clustered separately from each other on the uniform manifold approximation and projection (UMAP) even after 8 days in culture, including the two distinct clusters of homeostatic and ATM microglia. However, although cluster 1 of *in-vitro*-cultured microglia became simultaneously associated with the homeostatic and PVM microglia signature, suggesting that *in-vitro*-cultured microglia may attenuate some of the brain-associated specification and become more peripheral macrophage-like, some degree of separation between these two populations remained. This is consistent with previous findings that the tissue environment and cell ontology drive microglia specification and potentially explains why microglia signatures

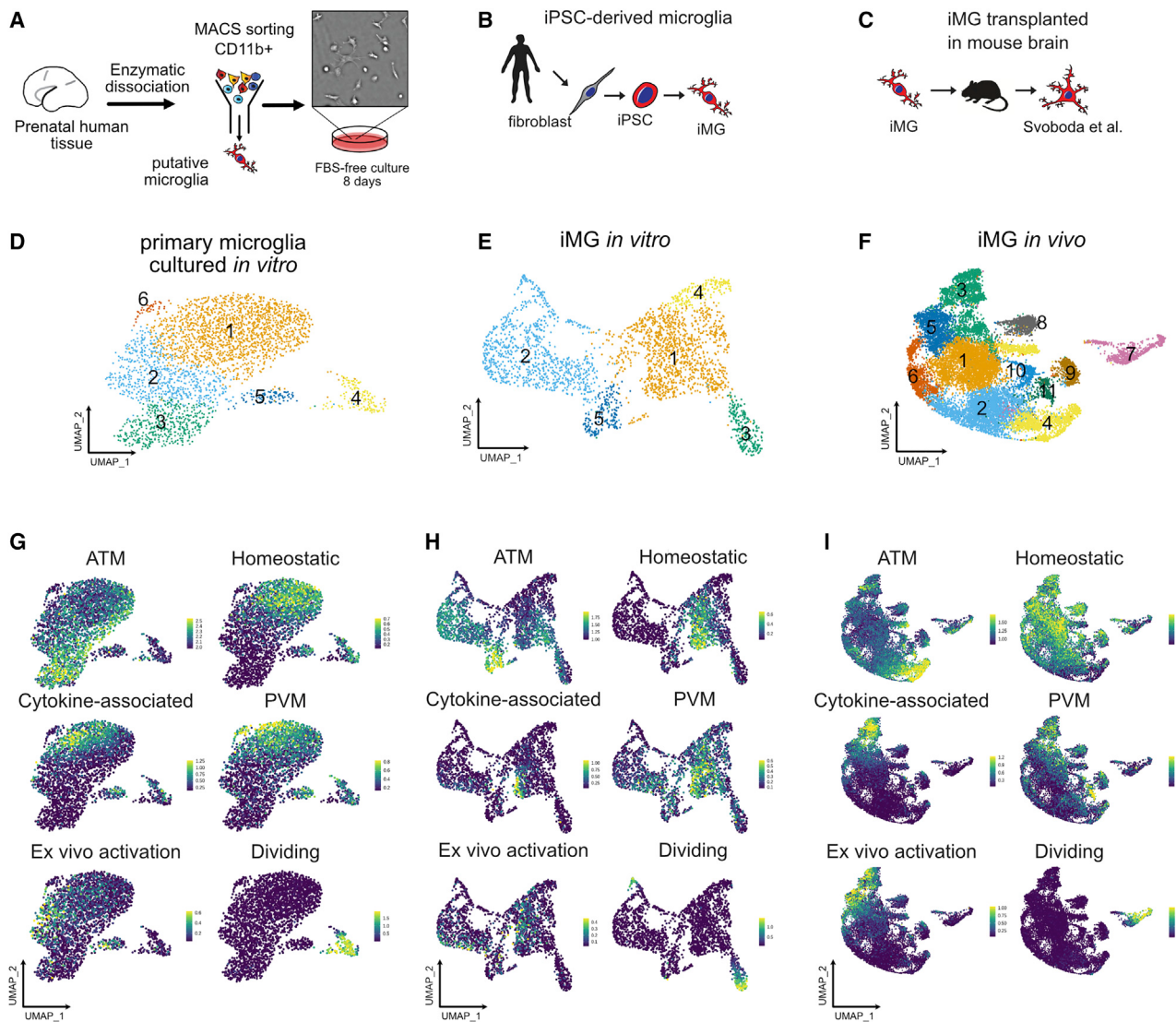


Figure 1. A developing brain microglia “report card” across culture models

(A) Primary human microglia were extracted from the mid-gestation human brain. The tissue was dissociated enzymatically with papain, MACS-sorted with Cd11b magnetic bead-conjugated antibody, and cultured in defined medium for 8 days.

(B) Microglia from induced pluripotent stem cells as a reliable microglia source. n = 1 (iCell Microglia, catalog number 01279).

(C) A schematic for induced microglia transplanted into the mouse brain (from Sloboda et al., 2019).

(D) UMAP plot of 2,970 microglia after 8 days of *in vitro* culture reveals five microglia clusters. n = 1 brain sample (GW23 primary cortex). See also Figure S1.

(E) scRNA-seq identifies six molecular clusters among induced microglia cells. 2,659 induced microglia (iMGs) cells from 1 experiment were used.

(F) scRNA-seq identifies eight molecular clusters among induced microglia cells “cultured” in the mouse brain. 15,971 cells from 4 mouse brain samples 60 days after injection were used, as described previously (Sloboda et al., 2019).

(G–I) Scores for individual microglia clusters for primary human microglia from Figures S1 and S2 were calculated and projected onto gene expression space for each microglia model. Individual genes used to calculate model scores are shown in Figure S2. ATM, axon tract-associated microglia (with high expression of *LGALS/LGALS3*, *APOC1*, and *SPP1*); homeostatic microglia, cluster with high expression of *CX3CR1*, *P2RY12/P2RY13*, *VSIR*, and *IFNGR1*; cytokine-associated microglia, cluster with high expression of *CCL3/CCL4*, *CXCL8*, *IL1B*, and *TNF*; PVM, perivascular macrophage (characterized by high expression of *F13A1*, *MRC1*, *LYVE1*, and *LYZ*); ex vivo activation, microglia cluster with high expression of genes associated with cell stress during enzymatic cell dissociation (*JUN*, *HSPA6/HSPA1A*, *DUSP1*, and *FOS*); dividing cells, cells characterized by cell cycle genes (*TOP2A*, *MKI67*, and *CENPF*).

See also Figure S1–S3 and Table S1.

can revert to their brain identity after being maintained under *ex vivo* conditions (Bennett et al., 2018). In contrast, microglia derived from iPSCs had a fully overlapping signature for homeostatic microglia and peripheral macrophages. These two populations became well separated again upon transplantation into the

mouse brain, suggesting that the initial minimal patterning cocktail to derive iMGs may still lack some of the signaling molecules that are unique to the brain parenchyma environment.

Consistent with previous reports, we found that human iMGs transplanted into the mouse brain recapitulated many of the

primary cell signatures and developed transcriptomic similarities with microglia in the human brain (Figure 1I; Figure S1C), suggesting that the neural tissue environment likely provides cues that support normal microglia identity (Bohlen et al., 2017). Individual module scores projected onto the UMAP revealed high preservation of microglia from the ATM cluster (Figure 1I). In contrast to the mouse brain transcriptomics data, where this cluster is transiently present in the early postnatal period of mouse development and then disappears at later time points (Hammond et al., 2019), our analysis suggests that human microglia retain this signature even in the adult mouse brain. Interesting, this cluster is characterized by high expression of *APOE* and *TREM2*, among others—two genes that are implicated in Alzheimer’s disease. Another cluster that was strongly preserved between primary and *in-vivo*-transplanted microglia was a cytokine-associated module that has been proposed previously to be specifically enriched in the human brain (Geirsdottir et al., 2019). This analysis revealed that, although *in vitro* culture decreases some of the key homeostatic microglia genes, it retains gene module specificity between different cell clusters. This specification is maintained and improved by xenotransplantation into the mouse brain. Two clusters (ATM and cytokine-associated) from *in-vivo*-transplanted microglia potentially uncover gene module signatures that, in human microglia, are maintained based on cell-intrinsic programs instead of relying on the brain tissue environment.

The “neuroimmune” organoid model of human brain development

The role of microglia in the early stages of human neurogenesis and neuronal maturation is a long-standing question because of the lack of experimental models. Given the extreme transcriptional plasticity of microglia and their sensitivity to the cell environment, we wondered whether seeding them into brain organoids could rescue the transcriptomics signatures of cultured microglia. *In vitro* differentiation protocols of human pluripotent stem cells are becoming widely adopted to derive cultured models of the developing brain (Figures 2A, 2B, and 2D; Figure S4A; Pasça, 2018). Unlike neurons, astrocytes, and oligodendrocytes, mature microglia do not emerge robustly in organoids derived by standard protocols but can be reconstituted by transplantation (Ormel et al., 2018). Combining 3D cortical organoids with exogenously derived microglia offers an opportunity to dissect the roles of this cell type in brain development. To this end, we differentiated human cortical brain organoids using standard protocols (Pasça et al., 2015), and at 5 weeks of differentiation, we introduced human microglia purified from mid-gestation cortical tissue specimens (Figure 2C). We selected this time period for transplantation because this is when the organoids are transferred to the final maintenance medium formulation that remains unchanged for the rest of the culture. Moreover, microglia do not actively proliferate in the organoids, whereas non-microglia progenitor cells do; therefore, we did not want to dilute the total proportion of microglia to non-microglia cells in the organoids. The resulting neuroimmune organoids were maintained in the organoid maintenance medium without any addition of trophic factors for microglia survival because our data suggest that different cell types present in the organoid express factors necessary for microglia survival, including IL-34

in excitatory neurons, CSF1 in radial glia, and TGF- β in dividing progenitor cells (<https://mg-models.cells.ucsc.edu>). Over the course of several days, microglia invaded the organoid (Videos S2 and S3) and transformed their morphology from an ameboid to a ramified state that could be detected even 5 weeks after engraftment (Figures 2E–2G; Figures S4B–S4D; Video S2). Similar results were obtained with microglia derived from iPSCs (Figures S4E–S4G). Microglia were located predominantly around rosettes with Sox2-positive neural stem cells, consistent with their role in the neurogenic niche of the developing mammalian brain (Figure S4H; Cunningham et al., 2013). The presence of microglia did not induce any macroscopic structural changes to the organoids (Figure S4J). We did not detect any Iba1-positive cells in any of the organoids that were not transplanted with microglia. Thus, the neuroimmune organoid offers an opportunity to explore the long-term effect of microglia on human neurogenesis and neuronal maturation.

A time-lapse imaging assay demonstrated that microglia were ramified with highly active motile processes, consistent with their surveillance function under homeostatic conditions (Figure 3A; Nimmerjahn et al., 2005). We also detected a subset of phagocytic microglia identified by the presence of phagocytic cups, protrusions of the plasma membrane engulfing nuclei of neighboring cells (Figure 3B). 3D reconstruction revealed that Sox2-positive progenitor cells can be found encapsulated by these phagocytic cups. Microglia additionally made contacts with Tuj1-positive neuronal fibers (Figure 3C). To examine whether microglia were actively phagocytosing synaptic material, consistent with their role *in vivo*, we performed additional staining for the microglial lysosome marker CD68. We detected synaptic material that was co-localized with microglial lysosomes (Figure 3D), and the overall volume of the engulfed synapse material was comparable with what is seen in the mouse brain (Figure 3E; Li et al., 2020).

Microglia in the 3D organoid environment

To investigate whether organoids can be used to preserve the homeostatic signatures of primary microglia or mature iMGs, we cultured primary human microglia in organoids for 2 weeks before performing scRNA-seq analysis (Figures 4A and 4B; Figure S5). After filtering non-microglia cells and iterative re-clustering, we identified 13 molecularly unique clusters. Our data suggest that, although the organoid environment increases the “homeostatic” score compared with 2D *in vitro*-cultured microglia, it also leads to an increase in the cytokine-associated signature to levels observed in primary uncultured microglia (Figure 4C). This cytokine-associated signature has been reported previously to be human specific (Geirsdottir et al., 2019), and a recent transcriptomics analysis of primary human microglia (Kracht et al., 2020), together with our own data, confirms the existence of this transcriptomic signature in normal microglia without any prior immune stimulation. In contrast to the human brain, the mouse microglia expression signatures of chemokines and *IL1B*, *CCL3*, and *CCL4* (also known as macrophage inflammatory protein-1b [Mip-1b]) emerge in the aged brain (Hammond et al., 2019). Our comparative analysis reveals that the mouse brain environment induces only moderate expression of the cytokine gene module, whereas human cortical organoids, representing a spectrum of cell types of

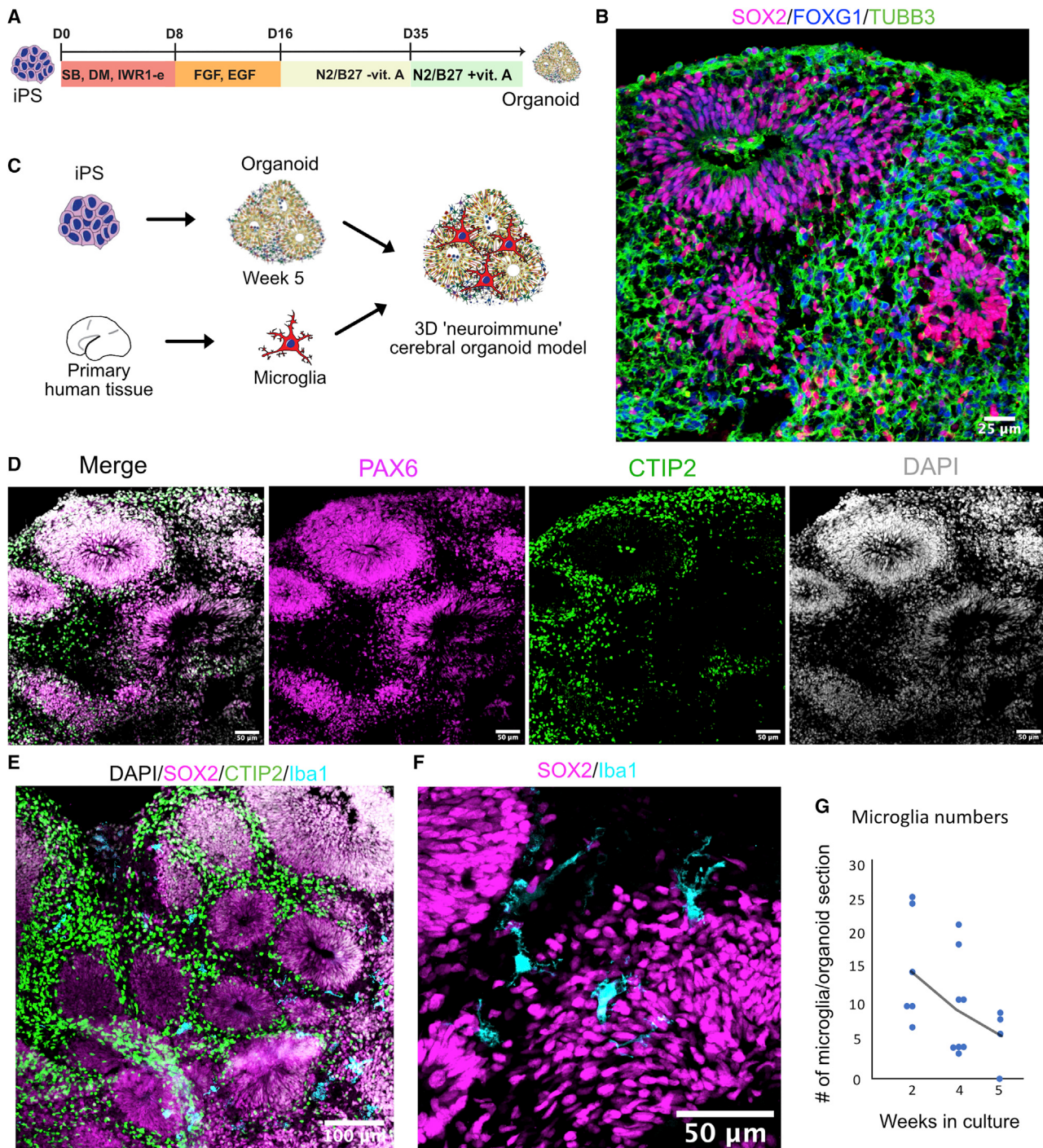


Figure 2. The neuroimmune organoid model of human brain development

- (A) Cortical organoids were generated and patterned using dual SMAD and Wnt inhibition. After day 35 in culture, cortical organoids were moved into a maintenance medium containing vitamin A and were maintained in the same medium for the duration of the experiment.
- (B) Cortical organoids express the forebrain marker FOXG1, the radial glia marker Sox2, and the pan-neuronal marker TUBB3.
- (C) Organoids were generated from iPSCs and, after switching to maintenance medium at 5 weeks, combined with primary human microglia to generate neuroimmune organoids.
- (D) Cortical organoids express markers for the cortical radial glial marker PAX6 and cortical layer 5 neuronal marker CTIP2.
- (E) Microglia are distributed throughout the organoid.
- (F) Iba1-positive microglia cells are ramified and distributed between and around rosettes.
- (G) Microglia numbers decrease monotonically over the 5-week co-culture time.

See also Figure S4.

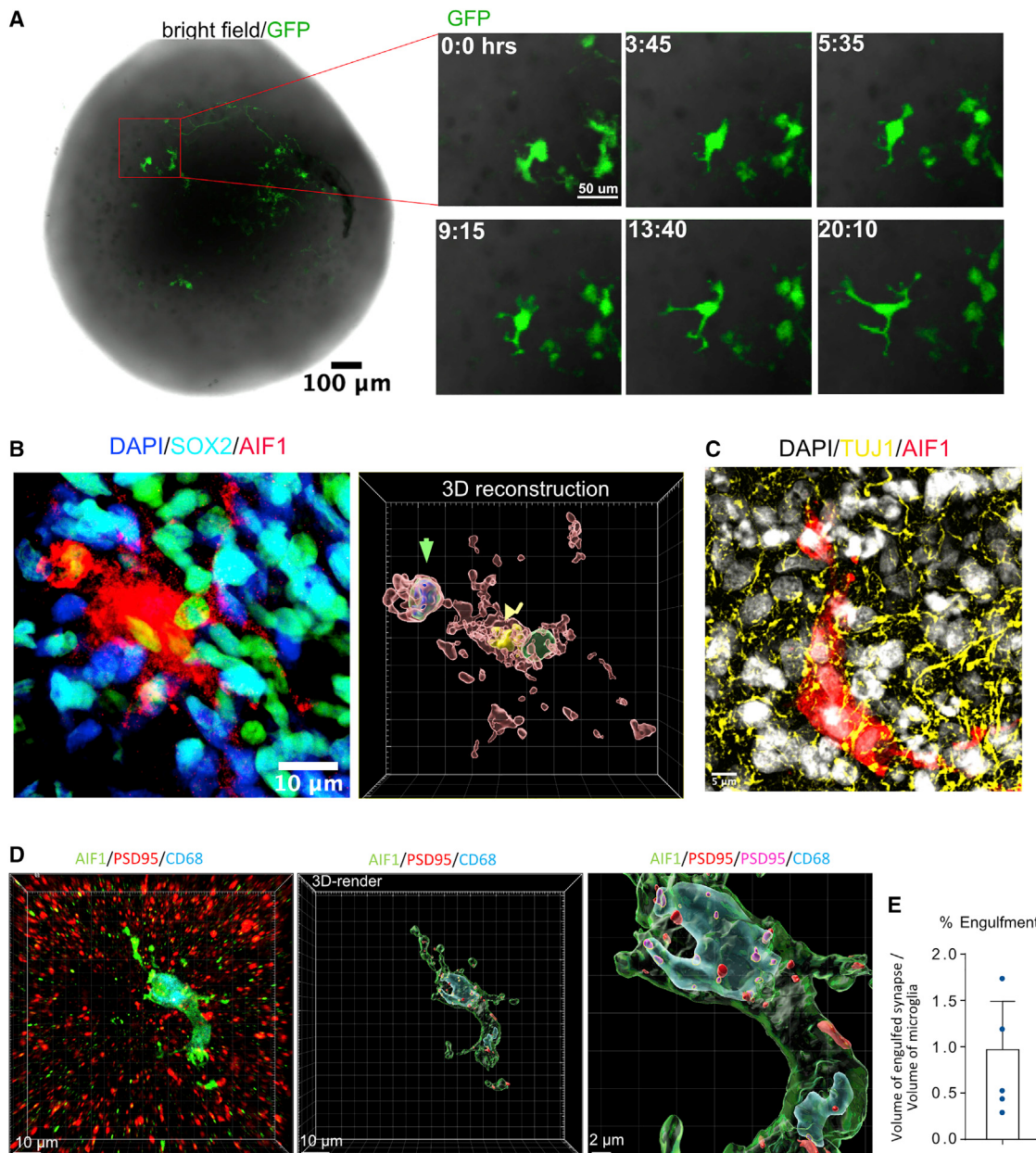


Figure 3. Microglia engrafted in organoids are motile and phagocytose progenitor cells and synaptic material

(A) Microglia are ramified and motile in the organoid. For time-lapse imaging, acutely purified microglia were labeled with adenovirus CMV-GFP and then engrafted into organoids. 7 days after integration, the organoid was imaged for 24 h to demonstrate the microglia's motile surveilling behavior. Virally labeled microglia were used only for the imaging experiments.

(B) Microglia in organoids form phagocytic cups containing Sox2-positive nuclei. Left: immunofluorescence labeling of a microglia cell (AIF1, red) and Sox2-positive organoid-resident radial glial cells (cyan). Right: 3D reconstruction of a Sox2-positive nucleus (green arrowhead) and microglia nucleus (yellow nucleus).

(C) Engrafted microglia (AIF1, red) surrounded by organoid-resident neuronal fibers (labeled with tuj1, yellow).

(D) Microglia (labeled with AIF1, in red) in an organoid stained with the lysosomal marker CD68 (in blue) demonstrates postsynaptic material (psd95; red) located in the lysosomes (psd95 overlapped with CD68; magenta).

(E) Volume of engulfed synapses normalized to the microglia volume. Error bar represents standard deviation. n = 5 individual organoids.

the developing human brain, are sufficient to restore the chemokine signature in microglia to the levels seen in the developing human brain. These data suggest that the chemokine signature may be associated specifically with the human brain environment and is downregulated significantly in the mouse

brain, reflecting the dynamic inducible nature of this microglia subtype/state (Figure 4C; Figure S5C).

In addition to the main signatures of the primary microglia (Figure 4C), we detected several populations of microglia that were only present in the organoid culture environment. Similar to the

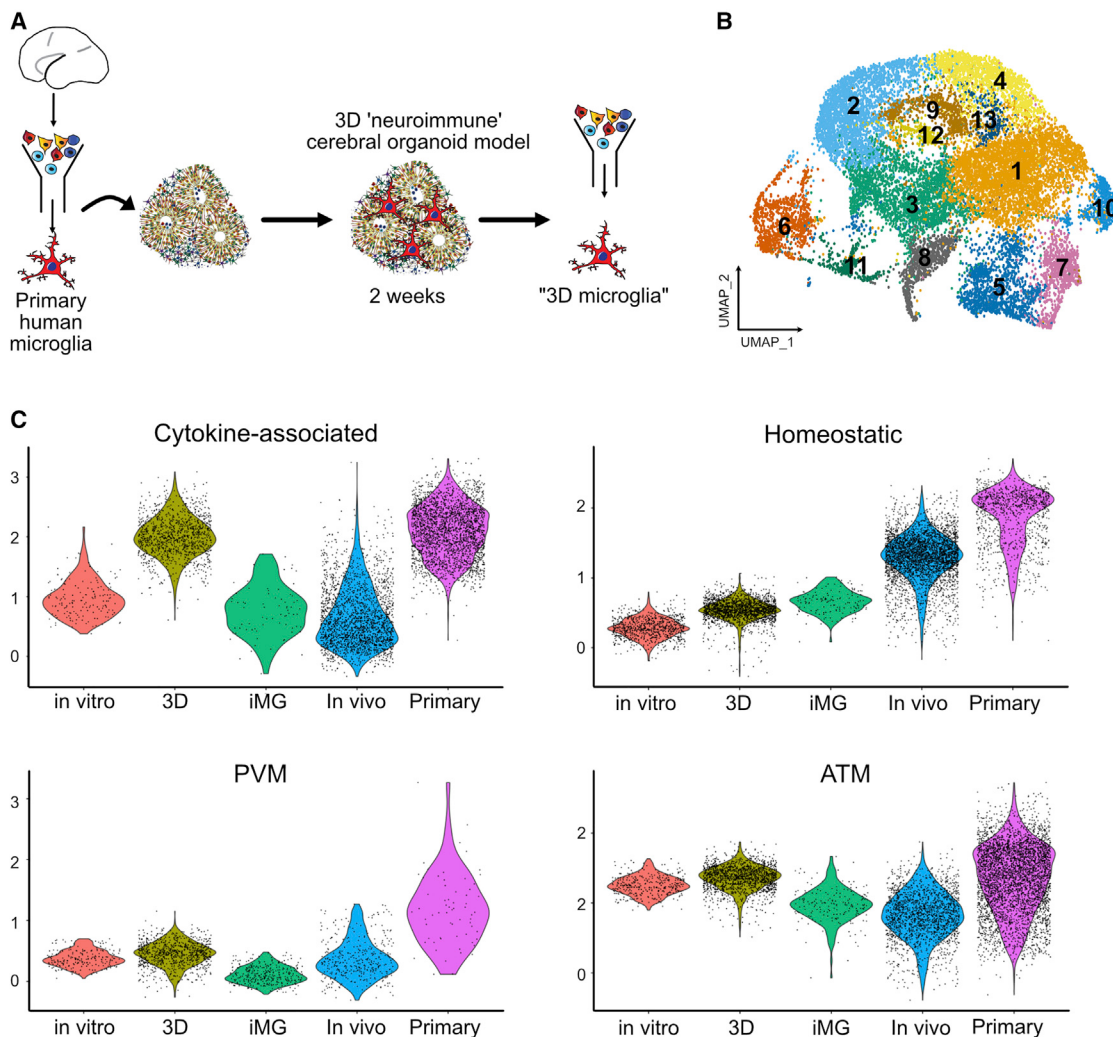


Figure 4. Microglia transplanted into organoids recapitulate primary human microglia

(A) Primary human microglia from human GW23 brain were purified using MACS CD11b beads and added to cortical organoids. Neuroimmune organoids were allowed to develop for 2 weeks, and then microglia cells were re-purified using CD11b magnetic beads for downstream scRNA-seq processing

(B) 17,705 microglia cells purified from organoids formed 13 clusters.

(C) Cross-model comparison of primary human microglia cultured *in vitro*, primary human microglia engrafted in cortical organoids (3D), induced microglia (iMGs), induced microglia transplanted into mouse brains (*in vivo*), and primary human microglia from mid-gestation from the BICC dataset.

See also Figure S5.

2D cultured cells, we identified a small population of microglia associated with the type I interferon response signaling gene signature (cluster 12; Figure S5B). We also identified a cluster with high expression of the metallothionein gene family (*MT1G*, *MT1H*, and *MT2A*) that was absent under any other model conditions. Metallothioneins are small proteins that are rich in cysteine residues, can bind multiple metals under physiological conditions, and are involved in heavy metal detoxification and redox regulation in the cells. In the brain, metallothionein expression is protective in response to injury and counteracts the effects of pro-inflammatory cytokines (Penkowa et al., 1999; Chung et al., 2009). High expression of these genes in organoid-cultured microglia may reflect their response to the cell stress of the organoid brain environment by upregulating the oxidate cell stress response (Bhaduri et al., 2020).

Human microglia reduce cell stress and attenuate interferon response genes

Given the strong transcriptomic signature that would be predicted to be protective, we wondered how the presence of microglia influences different cell types in the organoids. To systematically identify which transcriptomics signatures are differentially regulated among neural cells in the presence of microglia, neuroimmune organoids generated from three different iPSC lines were dissociated 5 weeks after transplantation and profiled using scRNA-seq. We identified the major cell types, including neurons, radial glia, intermediate progenitors, and dividing cells (Figures S6A–S6D). After selecting for cells of forebrain identity (FOXP1-positive), iterative clustering revealed the major cell types of the neuronal lineage, radial glia, intermediate progenitors, and dividing cells (Figure 5A; Figure S6E). Cells

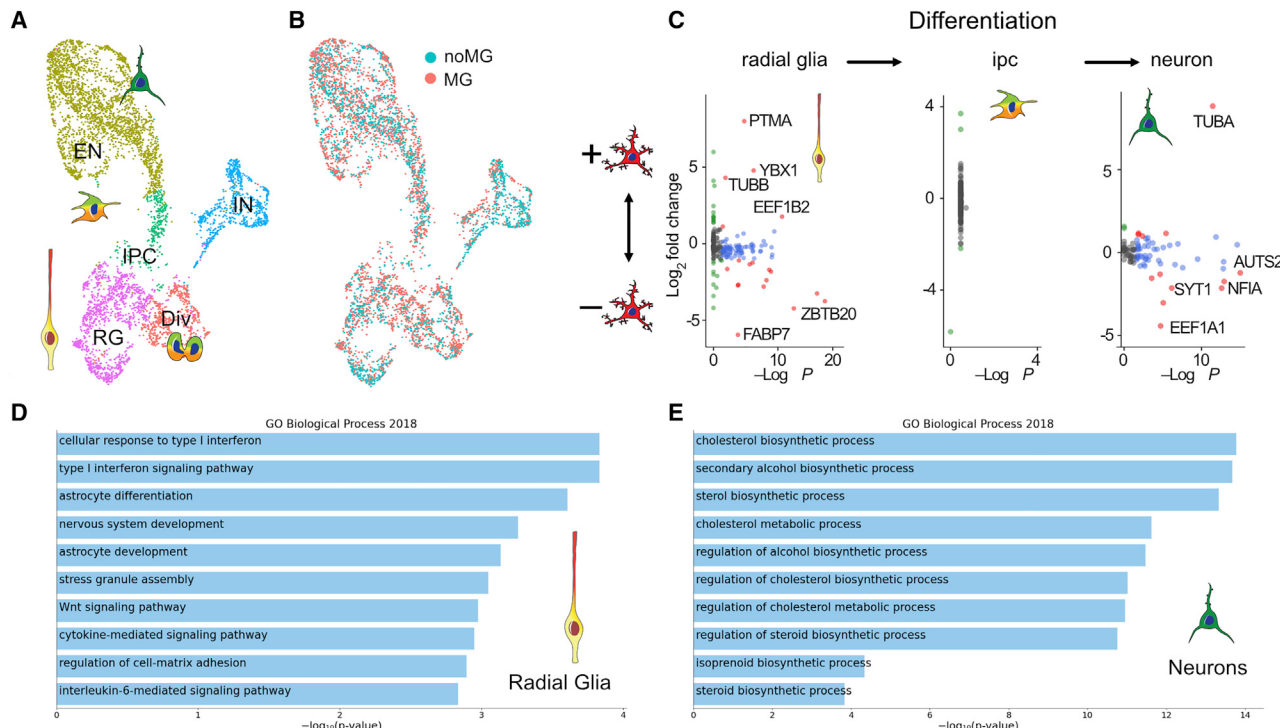


Figure 5. Microglia differentially regulate the gene expression profile in radial glia and neurons from cortical organoids

(A) scRNA-seq identifies main cell types in week 10 organoids. The UMAP plot is colored by clusters representing cell types. EN, excitatory neuron; IN, inhibitory neuron; IPC, intermediate progenitor cell; RG, radial glia cell; Div, dividing cell.

(B) UMAP of 5,507 cells colored by microglia presence or absence.

(C) Differentially expressed genes between control organoids and organoids transplanted with microglia.

(D) GO term analysis of the most affected genes in radial glia with an adjusted p value cutoff of 0.05. Radial glia from organoids transplanted with microglia downregulate genes in the interferon response pathway.

(E) Neurons from organoids transplanted with microglia upregulated genes in a lipid biosynthesis pathway

See also Figure S6 and Table S2.

derived from control and neuroimmune organoids as well as cells from all three organoid lines were found to be evenly distributed across all clusters (Figure 5B).

To uncover microglia-induced transcriptomic changes in each major cell type, we first calculated the amount of variance in expression level attributable to individual variables and selected genes with expression variation significantly contributed to by experimental condition (microglia-transplanted versus control organoids). Differential gene expression analysis revealed that radial glia and dividing cells are two top responding cell types to microglia (Figure 5C; Table S2). Among radial glial cells, gene set enrichment analysis using Enrichr (Chen et al., 2013) identified top biological processes associated with the presence of microglia, including a significant reduction in genes involved in metabolism as well as cellular response to interferon (Figure 5D). In contrast, fewer changes were identified in neurons. Among them, we observed genes involved in a cholesterol biosynthesis and acetyl-coenzyme A (CoA) pathway that were uniformly upregulated in response to the presence of microglia (Figure 5E; Figure S7D). Although we did not detect significant differences in individual gene expression in neurons with and without microglia, we noted some trends in expression of two genes associated with neuronal differentiation/maturation. Specifically, genes enriched in immature neurons, such as *NEUROD2*, were detected

at a higher average abundance in neurons derived from non-transplanted organoids. In contrast, genes typically expressed in more mature neurons, such as *NRXN1*, were enriched modestly in neurons derived from microglia-transplanted organoids (Figure S7E).

By focusing on the top differentially expressed genes from the interferon signaling pathway in radial glia in neuroimmune organoids, we identified several genes that were decreased markedly in the presence of microglia (Figure 6A; Figure S7A). Interferon regulatory factor 1 (*IRF1*), interferon alpha-inducible protein 6 (*IFI6*), interferon-induced transmembrane protein 3 (*IFITM3*), and human leukocyte antigen E (*HLA-E*) were among the top genes driving the gene ontology (GO) biological process analysis, and in the profiled organoids, this difference was specific to radial glial cells. We validated this difference by performing immunostaining in rosettes from neuroimmune organoids (Figure 6B). Co-staining with IFITM3 and Sox2 revealed a small but statistically significant decrease in IFITM3 levels in the presence of microglia, consistent with the transcriptomics data (Figures 6B and 6C; Figures S7F–S7H). Although the role of these changes at the level of radial glia cells in the human brain remains to be determined, it is interesting that *IFITM3*, one of the top interferon response genes identified in our analysis, is expressed robustly in human but not mouse radial glia cells (Figures S7B and S7C).

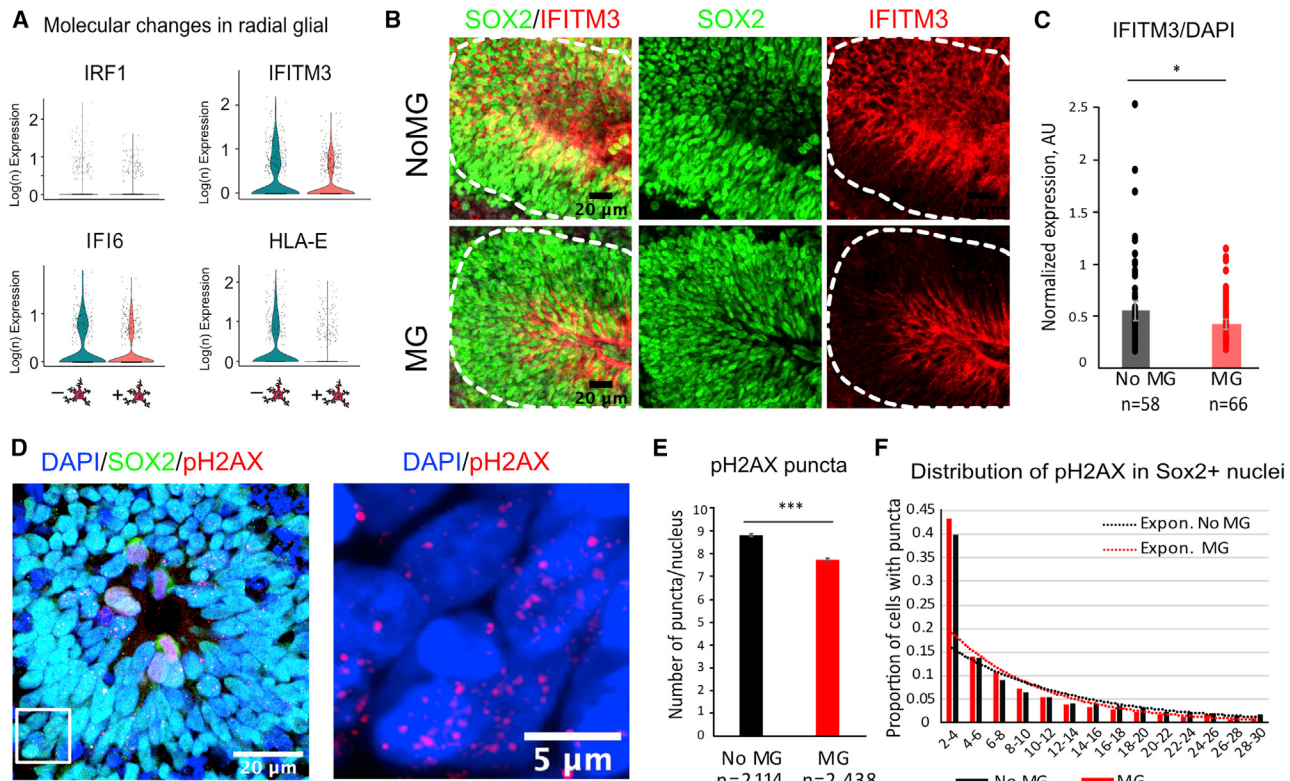


Figure 6. Human microglia attenuate the type I interferon response and decrease double-stranded DNA breaks in radial glia

- (A) Individual differentially expressed genes in organoids with and without microglia driving pathway analysis from Figure 5D.
- (B) Immunofluorescence validation of IFITM3 (interferon-induced transmembrane protein 3) in rosettes from organoids with and without microglia. The IFITM3 fluorescence signal was averaged across the rosette area (outlined in white).
- (C) IFITM3 has a small but statistically significant decrease in rosettes from organoids with microglia. $p < 0.05$. n are individual rosettes for each condition, quantified from sections from three independent organoids per condition. Error bars represent standard error of the mean.
- (D) An example of a rosette labeled with Sox2 for radial glial cells and a marker for double-stranded DNA breaks, pH2AX. A magnified window shows an example of cell nuclei with pH2AX puncta.
- (E) Averaged number of pH2AX puncta per cell nucleus. Cell nuclei with 2–30 pH2AX-positive puncta were used for analysis. $p < 0.001$. Number of nuclei for each condition are depicted on the graph.
- (F) Distribution of pH2AX number of puncta between conditions. Sox2-positive nuclei from microglia-transplanted organoids had a larger proportion of cells with fewer number of puncta. Organoids without microglia had a consistently higher proportion of cells with the number of puncta over 10.

See also Figure S7.

Although associated predominantly with immune defenses against various pathogenic stimuli, including viral infections, the interferon response is implicated in a general response to cellular stress, including DNA damage (Brzostek-Racine et al., 2011). Because our culture condition did not involve any viral challenge, we hypothesized that the interferon response pathway may be activated in response to cell stress induced by the organoid culture paradigm (Bhaduri et al., 2020). To test this hypothesis, we performed additional staining with pH2AX, a marker for double-stranded DNA breaks, and quantified the resulting puncta using CellProfiler (Jones et al., 2008). Among cell nuclei stained with Sox2 and pH2AX, we excluded ones with high levels of pH2AX, suggestive of dividing stem cells in the process of chromosome segregation (Turinotto and Giachino, 2015), and only quantified cells with 2–30 pH2AX-positive puncta (Figures 6D–6F). On average, the number of puncta per cell was greater in the absence of microglia. Distribution of nuclei with pH2AX-positive puncta revealed a trend with a higher proportion of cells

skewed toward a larger number of puncta per nucleus in control organoids, suggesting a small but significant and consistent increase in double-stranded DNA breaks in control organoids.

Microglia facilitate maturation of neural networks during brain development

It has been shown previously that microglia influence early network activity through physical contacts and secreted factors. In the scRNA-seq data, we detected a small but statistically significant change in expression of genes implicated in synaptic transmission. We sought to explore whether microglia might influence functional network maturation (Trujillo et al., 2019). To determine the effect of microglia on maturation of neural networks, we transplanted microglia into 15-week-old organoids, when the majority of neuronal types are expected to be present. We recorded spontaneous neural activity from the surface of the organoids using multi-electrode arrays (MEA) in neuroimmune and control organoids 5 weeks later (Figure 7A). Under both

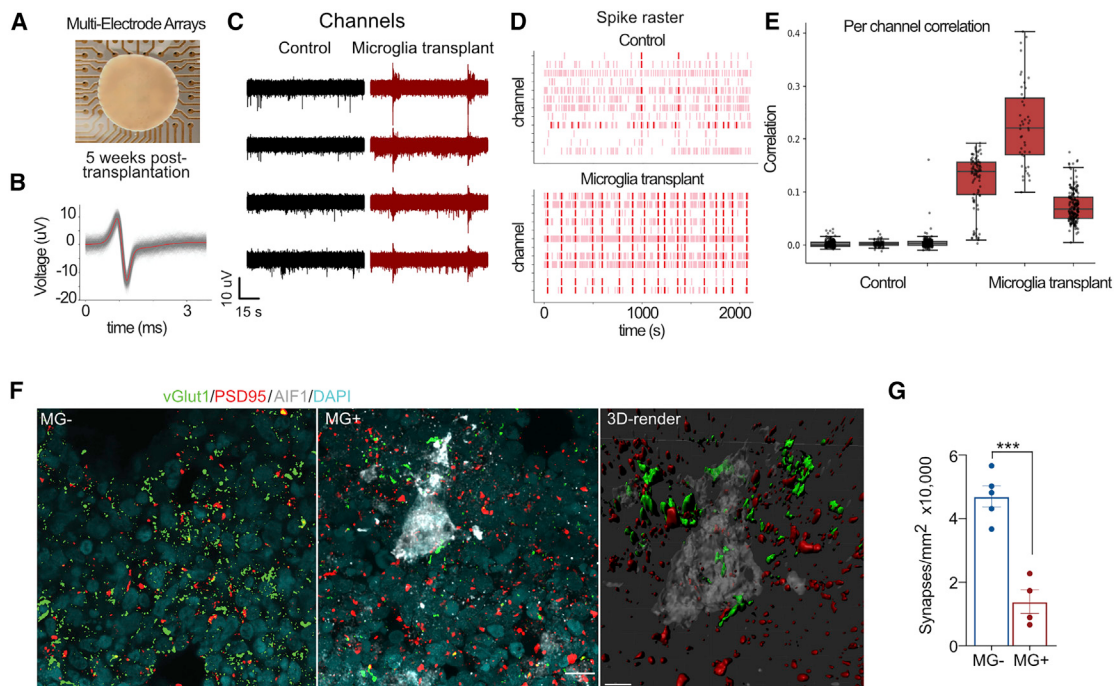


Figure 7. Microglia facilitate maturation of neural networks during brain development

- (A) Organoids transplanted with microglia were used for MEA recordings on a 64-electrode plate (Axion Biosystems).
- (B) An example of a single unit event. Individual events or “spikes” were overlaid on top of each other (gray), and the mean of these events is shown in red.
- (C) Representative traces for individual electrodes recorded from organoids without (black) and with (red) microglia.
- (D) Microglia transplantation promotes synchronized burst activity in cerebral organoids. Each pink line represents a spike that crossed the noise threshold (± 6 standard deviation), with red lines representing 10 or more spikes per second.
- (E) Microglia transplantation (in red) increases pairwise correlation between MEA electrodes compared with control (black) conditions. Each point represents one channel pair. Correlations are determined by binarizing activity in 40-ms bins. The box chart represents 25–75 percentile, with the horizontal line representing mean. The whiskers show the min and max values.
- (F) Microglia-transplanted organoids show reduced density of synapses.
- (G) Synapses were quantified based on co-localization of the presynaptic marker vGlut1 and postsynaptic marker psd95. The recordings were performed across three organoid lines with at least three fields of view per section. Data points represent the average of each organoid, and the bar chart represents the average of all fields of view for each condition. Error bars represent standard error of the mean. $p < 0.001$.

conditions, we detected spike activity with characteristic waveforms for single-unit activity (Figure 7B). We discovered increased synchronization and frequency of oscillatory bursts in neuroimmune organoids compared with the control (Figures 7C–7E), consistent with accelerated network maturation in organoids (Trujillo et al., 2019; Rigato et al., 2011; Parkhurst et al., 2013). To test the hypothesis that microglia are involved in synaptic refinement, we performed double immunostaining for vGlut1 and PSD95 and revealed a significant reduction in synaptic puncta, consistent with the role of microglia in synaptic remodeling, and we were able to detect synaptic material within microglia (Schafer et al., 2012; Weinhard et al., 2018; Figures 7F and 7G; Video S4). These findings suggest that microglia integrate into cerebral organoids, can be maintained within organoids for long-term culture, and contribute to development of functional neural networks.

DISCUSSION

We created a comprehensive comparison atlas among primary and iPSC-induced human microglia under different culture con-

ditions, including 2D culture and iMGs transplanted into mouse brains. We compared strategies for microglia culture that could serve as experimental systems for functional characterization of human microglia, including 2D culture and transplantation into cerebral organoids. To make this resource useful for the scientific community, we make it available via an interactive single cell browser (<https://mg-models.cells.ucsc.edu>). We show that, although the *in vivo* mouse brain environment significantly enhances fidelity of native microglia states, several important differences between iMGs and primary microglia still remain. First we show that a number of cytokine and chemokine genes is better preserved in a human-specific brain environment. It has been reported that the chemokine and cytokine signatures distinguish between mouse and human microglia (Geirsdottir et al., 2019), and we now show that the same gene modules remain downregulated in microglia transplanted into the mouse brain. This finding suggests that the native human brain environment may provide instructive cues for microglia development, perhaps reflecting deeper differences between the two species and further highlighting the effect of cell-cell interactions in shaping transcriptional and functional differences. In contrast, the ATM

microglia cluster is maintained under different culture conditions, including the mouse brain, suggesting that this microglia type may represent a stable microglia subtype.

Our research was motivated by two major questions. First, can brain organoids serve as a better culture environment for microglia, and second, can neuroimmune organoids become a more accurate model of the developing brain? To address these questions, we performed primary microglia transplantation into organoids, followed by scRNA-seq analysis of microglia and neural cells. Furthermore, we systematically characterized a neuroimmune model of 3D brain organoids transplanted with primary human microglia, and we show that microglia integrate into the organoids and affect brain development. By performing scRNA-seq analysis, we demonstrated that microglia transplanted in cerebral organoids had the closest resemblance to their *in vivo* counterparts. Furthermore, by comparing gene expression profiles between transplanted and control organoids, we detected subtle but statistically significant transcriptional differences in a cell-type-dependent manner. In radial glia, the presence of microglia reduces genes associated with the interferon response and their downstream effectors. Interestingly, expression of interferon genes is specific to radial glia in the human but not mouse brain, and activation of the interferon pathway regulates proliferation of human neural progenitors (Pereira et al., 2015). We attribute these changes to double-stranded DNA (dsDNA) damage that is enriched in long neural genes in neural stem and progenitor cells (Wei et al., 2016). Interestingly, increased DNA damage associated with increased neural progenitor proliferation has been associated with stress-susceptible genes, including ones implicated in autism spectrum disorder pathogenesis (Wang et al., 2020). Although the downstream effects of these gene expression differences and their connection to the pathogenesis of neurodevelopmental disorders are outside of the scope of this study, our work provides a roadmap for future hypothesis-based investigations into microglia-brain interactions.

In addition to identifying broad gene expression changes in microglia-containing organoids, our study reveals a role of microglia in neural circuit development. We detect an increase in network-level synchronized activity in microglia-containing organoids. This increase has been reported in maturing cortical organoids and was characteristic of developing cortical networks. Although several studies on microglia depletion in adult mouse brain have revealed a role of microglia in suppressing spontaneous activity and reducing seizures (Badimon et al., 2020; Merlini et al., 2021; Wu et al., 2020), the role of microglia in early circuit formation may differ from adult circuits. In postnatal mice, depletion of microglia leads to deficient synaptic pruning, accumulation of immature synapses, and weakening of functional connectivity (Zhan et al., 2014). Consistent with the role of microglia in phagocytic engulfment, we detected synaptic material in microglia cells and an overall reduction of synaptic puncta in microglia-transplanted organoids. However, we cannot exclude a role of microglia that is not associated with direct phagocytosis, such as release of soluble factors (Cheadle et al., 2020). We report a new neuroimmune model that can be used to investigate cell interactions between microglia and different cell types in the developing brain for disease modeling and that is amenable to therapeutic screening.

LIMITATIONS OF THE STUDY

Microglia numbers and cellular properties are tightly controlled in various brain regions. It has been shown previously that microglia from different brain regions differ in density, distribution, metabolism, and phagocytic/pruning behavior (Lawson et al., 1990; Tan et al., 2020). In our neuroimmune model, we noticed varying transplantation efficiency, with different organoids having different numbers of transplanted microglia. However, we did not notice any difference between different organoids at the level of single-cell transcriptome or protein expression levels. Our study is limited to cortical microglia transplanted into cortical organoids; therefore, performing transplantation using microglia isolated from different brain regions as well as employing organoids representing regional brain niches would be of great interest. Additionally, although human organoids are a good model for early brain development, they have not yet reached neural circuitry resembling a mature brain. In this study, we focused on a relatively short time period when neural circuits are just being developed. It would be important to see the effects of the absence of microglia at later time points. It has been previously reported that spontaneous networks with regular oscillatory events develop in organoids over their maturation trajectory (Trujillo et al., 2019). More work is needed to determine long-lasting microglia effects on different cell types in organoids.

STAR METHODS

Detailed methods are provided in the online version of this paper and include the following:

- **KEY RESOURCES TABLE**
- **RESOURCE AVAILABILITY**
 - Lead contact
 - Materials availability
 - Data and code availability
- **EXPERIMENTAL MODEL AND SUBJECT DETAILS**
 - Primary human samples
 - Sample size estimation
 - How subjects/samples were allocated to experimental groups
 - Health/immune status
 - Culture conditions for *in vitro* systems
- **METHOD DETAILS**
 - Time-lapse imaging of microglia in 2D culture
 - Time-lapse imaging of microglia in organoids
 - Organoid single-cell capture for single-cell RNA sequencing
 - Single cell RNA sequencing library preparation
 - Immunofluorescence
 - Axion recordings
- **QUANTIFICATION AND STATISTICAL ANALYSIS**
 - Single cell RNA sequencing Analysis
 - Differential Expression
 - Synapse quantification
 - IFITM3 quantification
 - pH2AX quantification
 - Axion data analysis
- **ADDITIONAL RESOURCES**

SUPPLEMENTAL INFORMATION

Supplemental information can be found online at <https://doi.org/10.1016/j.stem.2021.08.015>.

ACKNOWLEDGMENTS

We thank Drs. Aparna Bhaduri and Arnold Kriegstein for generously facilitating access to BICCN datasets. We thank all members of the Nowakowski, Mehta, and Piao laboratories for helpful discussions and comments throughout this project. This study was supported by gifts from Schmidt Futures and the William K. Bowes Jr. Foundation, a Simons Foundation grant (SFARI 491371 to T.J.N.), a Chan Zuckerberg Biohub Intercampus Investigator Award (to T.J.N.), NIH R01 NS083513 (to X.P.), NIH R01 NS108446 (to X.P.), NIH R01 NS118442 (to K.B.H.) and NIH NRSA F32 1F32MH118785 (to G.P.).

AUTHOR CONTRIBUTIONS

G.P. and T.J.N. contextualized the study. G.P. performed the experiments and analyzed the data. G.P. and C.N.K. formally analyzed the data. S.S.S. performed culture and immunofluorescence validation. B.B.C. provided *in vitro* microglia imaging experiments. C.S.M. and Z.J.G. provided resources and conceptual help with scRNA-seq experiments. K.M.H. performed the pH2AX staining quantification. D.T. and T.L. performed synapse imaging and quantification. S.J. performed induced microglia transplantation and quantification. M.G.K., D.S., and K.B.H. performed organoid multi-electrode array recordings and data analyses. S.B.M., X.P., R.R.R., and T.J.N. provided resources, designed the study, and provided conceptual feedback. G.P. and T.J.N. wrote the manuscript. All authors read and approved the manuscript.

DECLARATION OF INTERESTS

The authors declare no competing interests.

Received: December 21, 2020

Revised: June 23, 2021

Accepted: August 25, 2021

Published: September 17, 2021

SUPPORTING CITATIONS

The following references appear in the supplemental information: Nowakowski et al. (2017).

REFERENCES

- Abud, E.M., Ramirez, R.N., Martinez, E.S., Healy, L.M., Nguyen, C.H.H., Newman, S.A., Yeromin, A.V., Scarfone, V.M., Marsh, S.E., Fimbres, C., et al. (2017). iPSC-Derived Human Microglia-like Cells to Study Neurological Diseases. *Neuron* 94, 278–293.e9.
- Andreatta, M., and Carmona, S.J. (2021). UCell: robust and scalable single-cell gene signature scoring. *bioRxiv*. <https://doi.org/10.1101/2021.04.13.439670>.
- Badimon, A., Strasburger, H.J., Ayata, P., Chen, X., Nair, A., Ikegami, A., Hwang, P., Chan, A.T., Graves, S.M., Uweru, J.O., et al. (2020). Negative feedback control of neuronal activity by microglia. *Nature* 586, 417–423.
- Becht, E., McInnes, L., Healy, J., Dutertre, C.A., Kwok, I.W.H., Ng, L.G., Ginhoux, F., and Newell, E.W. (2018). Dimensionality reduction for visualizing single-cell data using t-SNE. *Nat. Biotechnol.* 37, 38–44.
- Bennett, F.C., Bennett, M.L., Yaqoob, F., Mulinyawe, S.B., Grant, G.A., Hayden Gephart, M., Plowey, E.D., and Barres, B.A. (2018). A Combination of Ontogeny and CNS Environment Establishes Microglial Identity. *Neuron* 98, 1170–1183.e8.
- Bernstein, N., Fong, N., Lam, I., Roy, M., Hendrickson, D.G., and Kelley, D.R. (2019). Solo: doublet identification via semi-supervised deep learning. *bioRxiv*. <https://doi.org/10.1101/841981>.
- Bershteyn, M., Nowakowski, T.J., Pollen, A.A., Di Lullo, E., Nene, A., Wynshaw-Boris, A., and Kriegstein, A.R. (2017). Human iPSC-Derived Cerebral Organoids Model Cellular Features of Lissencephaly and Reveal Prolonged Mitosis of Outer Radial Glia. *Cell Stem Cell* 20, 435–449.e434.
- Bhaduri, A., Andrews, M.G., Mancia Leon, W., Jung, D., Shin, D., Allen, D., Jung, D., Schmunk, G., Haeussler, M., Salma, J., et al. (2020). Cell stress in cortical organoids impairs molecular subtype specification. *Nature* 578, 142–148.
- Bohlen, C.J., Bennett, F.C., Tucker, A.F., Collins, H.Y., Mulinyawe, S.B., and Barres, B.A. (2017). Diverse Requirements for Microglial Survival, Specification, and Function Revealed by Defined-Medium Cultures. *Neuron* 94, 759–773.e8.
- Bortolotti, D., Gentili, V., Rotola, A., Caselli, E., and Rizzo, R. (2019). HHV-6A infection induces amyloid-beta expression and activation of microglial cells. *Alzheimers Res. Ther.* 11, 104.
- Brzostek-Racine, S., Gordon, C., Van Scyoc, S., and Reich, N.C. (2011). The DNA damage response induces IFN. *J. Immunol.* 187, 5336–5345.
- Butler, A., Hoffman, P., Smibert, P., Papalexi, E., and Satija, R. (2018). Integrating single-cell transcriptomic data across different conditions, technologies, and species. *Nat. Biotechnol.* 36, 411–420.
- Cheadle, L., Rivera, S.A., Phelps, J.S., Ennis, K.A., Stevens, B., Burkly, L.C., Lee, W.A., and Greenberg, M.E. (2020). Sensory Experience Engages Microglia to Shape Neural Connectivity through a Non-Phagocytic Mechanism. *Neuron* 108, 451–468.e9.
- Chen, E.Y., Tan, C.M., Kou, Y., Duan, Q., Wang, Z., Meirelles, G.V., Clark, N.R., and Ma'ayan, A. (2013). Enrichr: interactive and collaborative HTML5 gene list enrichment analysis tool. *BMC Bioinformatics* 14, 128.
- Chung, R.S., Leung, Y.K., Butler, C.W., Chen, Y., Eaton, E.D., Pankhurst, M.W., West, A.K., and Guillemin, G.J. (2009). Metallothionein treatment attenuates microglial activation and expression of neurotoxic quinolinic acid following traumatic brain injury. *Neurotox. Res.* 15, 381–389.
- Cunningham, C.L., Martínez-Cerdeño, V., and Noctor, S.C. (2013). Microglia regulate the number of neural precursor cells in the developing cerebral cortex. *J. Neurosci.* 33, 4216–4233.
- Finak, G., McDavid, A., Yajima, M., Deng, J., Gersuk, V., Shalek, A.K., Slichter, C.K., Miller, H.W., McElrath, M.J., Prlic, M., et al. (2015). MAST: a flexible statistical framework for assessing transcriptional changes and characterizing heterogeneity in single-cell RNA sequencing data. *Genome Biol.* 16, 278.
- Fleming, S.J., Marioni, J.C., and Babadi, M. (2019). CellBender remove-background: a deep generative model for unsupervised removal of background noise from scRNA-seq datasets. *bioRxiv*. <https://doi.org/10.1101/791699>.
- Gallego Romero, I., Pavlovic, B.J., Hernando-Herraez, I., Zhou, X., Ward, M.C., Banovich, N.E., Kagan, C.L., Burnett, J.E., Huang, C.H., Mitrano, A., et al. (2015). A panel of induced pluripotent stem cells from chimpanzees: a resource for comparative functional genomics. *eLife* 4, e07103.
- Garden, G.A. (2002). Microglia in human immunodeficiency virus-associated neurodegeneration. *Glia* 40, 240–251.
- Geirsdottir, L., David, E., Keren-Shaul, H., Weiner, A., Bohlen, S.C., Neuber, J., Balic, A., Giladi, A., Sheban, F., Dutertre, C.A., et al. (2019). Cross-Species Single-Cell Analysis Reveals Divergence of the Primate Microglia Program. *Cell* 179, 1609–1622.e16.
- Gosselin, D., Skola, D., Coufal, N.G., Holtzman, I.R., Schlachetzki, J.C.M., Sajti, E., Jaeger, B.N., O'Connor, C., Fitzpatrick, C., Pasillas, M.P., et al. (2017). An environment-dependent transcriptional network specifies human microglia identity. *Science* 356, eaai3222.
- Hafemeister, C., and Satija, R. (2019). Normalization and variance stabilization of single-cell RNA-seq data using regularized negative binomial regression. *Genome Biol.* 20, 296.
- Hammond, T.R., Dufort, C., Dissing-Olesen, L., Giera, S., Young, A., Wysoker, A., Walker, A.J., Gergits, F., Segel, M., Nemesh, J., et al. (2019). Single-Cell RNA Sequencing of Microglia throughout the Mouse Lifespan and in the Injured Brain Reveals Complex Cell-State Changes. *Immunity* 50, 253–271.e6.
- Jones, T.R., Kang, I.H., Wheeler, D.B., Lindquist, R.A., Papallo, A., Sabatini, D.M., Golland, P., and Carpenter, A.E. (2008). CellProfiler Analyst: data exploration and analysis software for complex image-based screens. *BMC Bioinformatics* 9, 482.

- Keren-Shaul, H., Spinrad, A., Weiner, A., Matcovitch-Natan, O., Dvir-Szternfeld, R., Ulland, T.K., David, E., Baruch, K., Lara-Astaiso, D., Toth, B., et al. (2017). A Unique Microglia Type Associated with Restricting Development of Alzheimer's Disease. *Cell* 169, 1276–1290.e17.
- Korsunsky, I., Millard, N., Fan, J., Slowikowski, K., Zhang, F., Wei, K., Baglaenko, Y., Brenner, M., Loh, P.R., and Raychaudhuri, S. (2019). Fast, sensitive and accurate integration of single-cell data with Harmony. *Nat. Methods* 16, 1289–1296.
- Kracht, L., Borggrewe, M., Eskandar, S., Brouwer, N., Chuva de Sousa Lopes, S.M., Laman, J.D., Scherjon, S.A., Prins, J.R., Kooistra, S.M., and Eggen, B.J.L. (2020). Human fetal microglia acquire homeostatic immune-sensing properties early in development. *Science* 369, 530–537.
- Krasemann, S., Madore, C., Cialic, R., Baufeld, C., Calcagno, N., El Fatimy, R., Beckers, L., O'Loughlin, E., Xu, Y., Fanek, Z., et al. (2017). The TREM2-APOE Pathway Drives the Transcriptional Phenotype of Dysfunctional Microglia in Neurodegenerative Diseases. *Immunity* 47, 566–581.e9.
- Kreitzer, F.R., Salomonis, N., Sheehan, A., Huang, M., Park, J.S., Spindler, M.J., Lizarraga, P., Weiss, W.A., So, P.L., and Conklin, B.R. (2013). A robust method to derive functional neural crest cells from human pluripotent stem cells. *Am. J. Stem Cells* 2, 119–131.
- Lawson, L.J., Perry, V.H., Dri, P., and Gordon, S. (1990). Heterogeneity in the distribution and morphology of microglia in the normal adult mouse brain. *Neuroscience* 39, 151–170.
- Lehrman, E.K., Wilton, D.K., Litvina, E.Y., Welsh, C.A., Chang, S.T., Frouin, A., Walker, A.J., Heller, M.D., Umemori, H., Chen, C., and Stevens, B. (2018). CD47 Protects Synapses from Excess Microglia-Mediated Pruning during Development. *Neuron* 100, 120–134.e6.
- Li, Q., Cheng, Z., Zhou, L., Darmanis, S., Neff, N.F., Okamoto, J., Gulati, G., Bennett, M.L., Sun, L.O., Clarke, L.E., et al. (2019). Developmental Heterogeneity of Microglia and Brain Myeloid Cells Revealed by Deep Single-Cell RNA Sequencing. *Neuron* 101, 207–223.e10.
- Li, T., Chiou, B., Gilman, C.K., Luo, R., Koshi, T., Yu, D., Oak, H.C., Giera, S., Johnson-Venkatesh, E., Muthukumar, A.K., et al. (2020). A splicing isoform of GPR56 mediates microglial synaptic refinement via phosphatidylserine binding. *EMBO J.* 39, e104136.
- Marsh, S.E., Kamath, T., Walker, A.J., Dissing-Olesen, L., Hammond, T.R., Young, A.M.H., Abdulaouf, A., Nadaf, N., Dufort, C., Murphy, S., et al. (2020). Single Cell Sequencing Reveals Glial Specific Responses to Tissue Processing & Enzymatic Dissociation in Mice and Humans. *bioRxiv*. <https://doi.org/10.1101/2020.2020.2003.408542>.
- Masuda, T., Sankowski, R., Staszewski, O., Böttcher, C., Amann, L., Sagar, C., Scheiwe, C., Nessler, S., Kunz, P., van Loo, G., et al. (2019). Spatial and temporal heterogeneity of mouse and human microglia at single-cell resolution. *Nature* 566, 388–392.
- Matsumoto, Y., Hayashi, Y., Schlieve, C.R., Ikeya, M., Kim, H., Nguyen, T.D., Sami, S., Baba, S., Barruet, E., Nasu, A., et al. (2013). Induced pluripotent stem cells from patients with human fibrodysplasia ossificans progressiva show increased mineralization and cartilage formation. *Orphanet J. Rare Dis.* 8, 190.
- McGinnis, C.S., Patterson, D.M., Winkler, J., Conrad, D.N., Hein, M.Y., Srivastava, V., Hu, J.L., Murrow, L.M., Weissman, J.S., Werb, Z., et al. (2019). MULTI-seq: sample multiplexing for single-cell RNA sequencing using lipid-tagged indices. *Nat. Methods* 16, 619–626.
- McQuin, C., Goodman, A., Chernyshev, V., Kamentsky, L., Cimini, B.A., Karhohs, K.W., Doan, M., Ding, L., Rafelski, S.M., Thirstrup, D., et al. (2018). CellProfiler 3.0: Next-generation image processing for biology. *PLoS Biol.* 16, e2005970.
- Merlini, M., Rafalski, V.A., Ma, K., Kim, K.Y., Bushong, E.A., Rios Coronado, P.E., Yan, Z., Mendiola, A.S., Sozmen, E.G., Ryu, J.K., et al. (2021). Microglial Gi-dependent dynamics regulate brain network hyperexcitability. *Nat. Neurosci.* 24, 19–23.
- Montilla, A., Zabala, A., Matute, C., and Domercq, M. (2020). Functional and Metabolic Characterization of Microglia Culture in a Defined Medium. *Front. Cell. Neurosci.* 14, 22.
- Needleman, L.A., and McAllister, A.K. (2012). The major histocompatibility complex and autism spectrum disorder. *Dev. Neurobiol.* 72, 1288–1301.
- Nimmerjahn, A., Kirchhoff, F., and Helmchen, F. (2005). Resting microglial cells are highly dynamic surveillants of brain parenchyma in vivo. *Science* 308, 1314–1318.
- Nowakowski, T.J., Bhaduri, A., Pollen, A.A., Alvarado, B., Mostajo-Radji, M.A., Di Lullo, E., Haessler, M., Sandoval-Espinosa, C., Liu, S.J., Velmeshev, D., et al. (2017). Spatiotemporal gene expression trajectories reveal developmental hierarchies of the human cortex. *Science* 358, 1318–1323.
- Oosterhof, N., Chang, I.J., Karimiani, E.G., Kuil, L.E., Jensen, D.M., Daza, R., Young, E., Astle, L., van der Linde, H.C., Shivaram, G.M., et al. (2019). Homozygous Mutations in CSF1R Cause a Pediatric-Onset Leukoencephalopathy and Can Result in Congenital Absence of Microglia. *Am. J. Hum. Genet.* 104, 936–947.
- Ormel, P.R., Vieira de Sá, R., van Bodegraven, E.J., Karst, H., Harschnitz, O., Sneepoer, M.A.M., Johansen, L.E., van Dijk, R.E., Scheefhals, N., Berdenis van Berlekam, A., et al. (2018). Microglia innately develop within cerebral organoids. *Nat. Commun.* 9, 4167.
- Parkhurst, C.N., Yang, G., Ninan, I., Savas, J.N., Yates, J.R., 3rd, Lafaille, J.J., Hempstead, B.L., Littman, D.R., and Gan, W.B. (2013). Microglia promote learning-dependent synapse formation through brain-derived neurotrophic factor. *Cell* 155, 1596–1609.
- Paşca, S.P. (2018). The rise of three-dimensional human brain cultures. *Nature* 553, 437–445.
- Paşca, A.M., Sloan, S.A., Clarke, L.E., Tian, Y., Makinson, C.D., Huber, N., Kim, C.H., Park, J.Y., O'Rourke, N.A., Nguyen, K.D., et al. (2015). Functional cortical neurons and astrocytes from human pluripotent stem cells in 3D culture. *Nat. Methods* 12, 671–678.
- Penkowa, M., Carrasco, J., Giralt, M., Moos, T., and Hidalgo, J. (1999). CNS wound healing is severely depressed in metallothionein I- and II-deficient mice. *J. Neurosci.* 19, 2535–2545.
- Pereira, L., Medina, R., Baena, M., Planas, A.M., and Pozas, E. (2015). IFN gamma regulates proliferation and neuronal differentiation by STAT1 in adult SVZ niche. *Front. Cell. Neurosci.* 9, 270.
- Rademakers, R., Baker, M., Nicholson, A.M., Rutherford, N.J., Finch, N., Soto-Ortala, A., Lash, J., Wider, C., Wojtas, A., DeJesus-Hernandez, M., et al. (2011). Mutations in the colony stimulating factor 1 receptor (CSF1R) gene cause hereditary diffuse leukoencephalopathy with spheroids. *Nat. Genet.* 44, 200–205.
- Retallack, H., Di Lullo, E., Arias, C., Knopp, K.A., Laurie, M.T., Sandoval-Espinosa, C., Mancia Leon, W.R., Krencik, R., Ullian, E.M., Spatazza, J., et al. (2016). Zika virus cell tropism in the developing human brain and inhibition by azithromycin. *Proc. Natl. Acad. Sci. USA* 113, 14408–14413.
- Rigato, C., Buckinx, R., Le-Corronc, H., Rigo, J.M., and Legendre, P. (2011). Pattern of invasion of the embryonic mouse spinal cord by microglial cells at the time of the onset of functional neuronal networks. *Glia* 59, 675–695.
- Schafer, D.P., Lehrman, E.K., Kautzman, A.G., Koyama, R., Mardinaly, A.R., Yamasaki, R., Ransohoff, R.M., Greenberg, M.E., Barres, B.A., and Stevens, B. (2012). Microglia sculpt postnatal neural circuits in an activity and complement-dependent manner. *Neuron* 74, 691–705.
- Schindelin, J., Arganda-Carreras, I., Frise, E., Kaynig, V., Longair, M., Pietzsch, T., Preibisch, S., Rueden, C., Saalfeld, S., Schmid, B., et al. (2012). Fiji: an open-source platform for biological-image analysis. *Nat. Methods* 9, 676–682.
- Sekar, A., Bialas, A.R., de Rivera, H., Davis, A., Hammond, T.R., Kamitaki, N., Tooley, K., Presumey, J., Baum, M., Van Doren, V., et al.; Schizophrenia Working Group of the Psychiatric Genomics Consortium (2016). Schizophrenia risk from complex variation of complement component 4. *Nature* 530, 177–183.
- Svoboda, D.S., Barrasa, M.I., Shu, J., Rietjens, R., Zhang, S., Mitalipova, M., Berube, P., Fu, D., Shultz, L.D., Bell, G.W., and Jaenisch, R. (2019). Human iPSC-derived microglia assume a primary microglia-like state after transplantation into the neonatal mouse brain. *Proc. Natl. Acad. Sci. USA* 116, 25293–25303.

- Tan, Y.L., Yuan, Y., and Tian, L. (2020). Microglial regional heterogeneity and its role in the brain. *Mol. Psychiatry* 25, 351–367.
- Traag, V.A., Waltman, L., and van Eck, N.J. (2019). From Louvain to Leiden: guaranteeing well-connected communities. *Sci. Rep.* 9, 5233.
- Trujillo, C.A., Gao, R., Negraes, P.D., Gu, J., Buchanan, J., Preissl, S., Wang, A., Wu, W., Haddad, G.G., Chaim, I.A., et al. (2019). Complex Oscillatory Waves Emerging from Cortical Organoids Model Early Human Brain Network Development. *Cell Stem Cell* 25, 558–569.e7.
- Turinetto, V., and Giachino, C. (2015). Multiple facets of histone variant H2AX: a DNA double-strand-break marker with several biological functions. *Nucleic Acids Res.* 43, 2489–2498.
- Wang, M., Wei, P.C., Lim, C.K., Gallina, I.S., Marshall, S., Marchetto, M.C., Alt, F.W., and Gage, F.H. (2020). Increased Neural Progenitor Proliferation in a hiPSC Model of Autism Induces Replication Stress-Associated Genome Instability. *Cell Stem Cell* 26, 221–233.e6.
- Wei, P.C., Chang, A.N., Kao, J., Du, Z., Meyers, R.M., Alt, F.W., and Schwer, B. (2016). Long Neural Genes Harbor Recurrent DNA Break Clusters in Neural Stem/Progenitor Cells. *Cell* 164, 644–655.
- Weinhard, L., di Bartolomei, G., Bolasco, G., Machado, P., Schieber, N.L., Neniskyte, U., Exiga, M., Vadisiute, A., Raggioli, A., Schertel, A., et al. (2018). Microglia remodel synapses by presynaptic trogocytosis and spine head filopodia induction. *Nat. Commun.* 9, 1228.
- Wu, W., Li, Y., Wei, Y., Bosco, D.B., Xie, M., Zhao, M.G., Richardson, J.R., and Wu, L.J. (2020). Microglial depletion aggravates the severity of acute and chronic seizures in mice. *Brain Behav. Immun.* 89, 245–255.
- Zeisel, A., Muñoz-Manchado, A.B., Codeluppi, S., Lönnérberg, P., La Manno, G., Juréus, A., Marques, S., Munguba, H., He, L., Betsholtz, C., et al. (2015). Brain structure. Cell types in the mouse cortex and hippocampus revealed by single-cell RNA-seq. *Science* 347, 1138–1142.
- Zhan, Y., Paolicelli, R.C., Sforazzini, F., Weinhard, L., Bolasco, G., Pagani, F., Vyssotski, A.L., Bifone, A., Gozzi, A., Ragazzino, D., and Gross, C.T. (2014). Deficient neuron-microglia signaling results in impaired functional brain connectivity and social behavior. *Nat. Neurosci.* 17, 400–406.
- Zhong, S., Ding, W., Sun, L., Lu, Y., Dong, H., Fan, X., Liu, Z., Chen, R., Zhang, S., Ma, Q., et al. (2020). Decoding the development of the human hippocampus. *Nature* 577, 531–536.

STAR★METHODS

KEY RESOURCES TABLE

REAGENT or RESOURCE	SOURCE	IDENTIFIER
Antibodies		
CD68	Abcam	Abcam Cat# ab955, RRID:AB_307338
CTIP2	Abcam	Cat# ab18465, RRID:AB_2064130
EOMES	R&D Systems	Cat# AF6166, RRID:AB_10569705
FOXG1	Abcam	Cat# ab196868, RRID:AB_2892604
Iba1	Synaptic Systems	Cat# 234 004, RRID:AB_2493179
Iba1	Wako	Cat# 019-19741, RRID:AB_839504
IFITM3	Proteintech	Cat# 11714-1-AP, RRID:AB_2295684
Ki67	Agilent	Cat# M724001-2, RRID:AB_2631211
P2RY12	Sigma Aldrich	Cat# HPA014518, RRID:AB_2669027
PAX6	BioLegend	Cat# 901301, RRID:AB_2565003
pH2AX	Cell Signaling Technologies	Cat# 9718, RRID:AB_2118009
psd95	Thermo Fisher	Cat# 51-6900, RRID:AB_2533914
SATB2	Santa Cruz Biotechnology	Cat# sc-81376, RRID:AB_1129287
SOX2	Santa Cruz Biotechnology	Cat# sc-17320, RRID:AB_2286684
Tuj1	Biolegend	Cat# 80120, RRID:AB_2313773
VGLUT1	Millipore Sigma	Cat# MAB5502, RRID:AB_262185
Bacterial and viral strains		
AV-CMV-GFP	Vector Biolabs	1060
Chemicals, peptides, and recombinant proteins		
Antibiotic-Antimycotic	GIBCO	15240-062
B27 supplement w/o Vitamin A	GIBCO	12587-001
B27 w/ Vitamin A	GIBCO	17504-001
BDNF	Alomone	b250
CD lipid concentrate	Thermo Fisher	11905031
CellTracker CM-Dil	Thermo Fisher	C7000
DAPI Fluoromount	Southern Biotech	0100-20
DMEM/F12 with Glutamax	GIBCO	10565042
Dnase	Sigma Aldrich	DN25
Donkey Serum	Jackson Immuno	017-000-121
Dorsomorphin	Sigma-Aldrich	P5499
DPBS	GIBCO	14190250
Eagle's basal medium	UCSF Media Production Core	N/A
EGF	Peprotech	100-47
FBS	HyClone	SH30071.03
Fibronectin	Corning	354008
FGFb	Peprotech	100-18B
GlutaMax Supplement	Thermo Fisher Scientific	35050061
HBSS	UCSF Media Production Core	N/A
Human Insulin	Sigma	I2643-50MG
IL34	Peprotech	200-34
Insulin-Transferrin-Selenium (ITS-G) (100 ×)	Thermo Fisher Scientific	41400045
IWR1-ε	Cayman Chemical	13659
Laminin	Thermo Fisher	23017015
Matrigel	Fisher Scientific	354234

(Continued on next page)

Continued

REAGENT or RESOURCE	SOURCE	IDENTIFIER
N2 supplement	GIBCO	17502-048
Neurobasal	GIBCO	21103049
Non-essential Amino Acids (NEAA)	Thermo Fisher Scientific	11140050
PBS-EDTA, pH 7.5	Lonza	BE02-017F
Trypsin, 2.5%	GIBCO	15090046
Trypsin, 0.25%	Thermo Fisher	25200056
Critical commercial assays		
10X Chromium V2	10X Genomics	PN-120237
10X Chromium V3	10X Genomics	PN-1000092
Cd11b magnetic beads	Miltenyi Biotec	130-049-601
Experimental models: Cell lines		
Human iPS cell line 28126 (male)	Gilad Lab (Gallego Romero et al., 2015)	
Human iPS cell line “WTC-11” (male)	Conklin Lab (Bershteyn et al., 2017; Kreitzer et al., 2013)	CVCL_Y803
Human iPS cell line “1323-4” (female)	Conklin Lab (Matsumoto et al., 2013)	CVCL_0G84
Human iPS cell line “WTC-10” (male)	Conklin Lab (Bershteyn et al., 2017; Kreitzer et al., 2013)	
Human iMG	Fujifilm Cellular Dynamics	01279
Software and algorithms		
ImageJ (Fiji)	Schindelin et al., 2012	https://imagej.net/software/fiji
CellRanger v3.0	10X Genomics	https://support.10xgenomics.com/single-cell-gene-expression/software/pipelines/latest/what-is-cell-ranger
Seurat v3.0	Satija Lab (Butler et al., 2018)	https://satijalab.org/seurat/
deMULTIplex	Gartner Lab (McGinnis et al., 2019)	https://github.com/chris-mcginnis-ucsf/MULTI-seq
CellProfiler 3.0	McQuin et al., 2018	https://cellprofiler.org/
CellBender	Fleming et al., 2019	https://github.com/broadinstitute/CellBender
UCell	Andreatta and Carmona, 2021	https://github.com/carmonalab/UCell
Deposited data		
Primary microglia BICCN scRNaseq	Brain Initiative Cell Census Network	NeMO archive: RRID:SCR_015820
Primary microglia <i>in vitro</i> culture scRNaseq	This study	Synapse: syn26009957
Primary microglia in organoids scRNaseq	This study	Synapse: syn26009957
Induced microglia scRNaseq	This study	GEO: GSE180945
Organoids scRNaseq	This study	GEO: GSE180945
Microglia in mouse brain scRNaseq	Svoboda et al., 2019	GEO: GSE139194
Other		
6-well Ultralow Attachment Plates	Corning	3471
40 µm cell strainer	Corning	352340
LS columns	Miltenyi Biotec	130-042-401
glass-bottom 24 well plates	Cellvis	P24-1.5H-N
glass-bottom six-well plate	Mattek	P06G-1.5-10-F

RESOURCE AVAILABILITY**Lead contact**

Further information and requests for resources and reagents should be directed to and will be fulfilled by the lead contact, Tomasz J. Nowakowski, tomasz.nowakowski@ucsf.edu.

Materials availability

This study did not generate new unique reagents.

Data and code availability

Single-cell RNA-seq data for non-human data have been deposited at GEO (GEO: GSE180945) and are publicly available as of the date of publication. Newly generated single-cell RNA-seq data from de-identified human subjects has been deposited at Synapse (Synapse: <https://www.synapse.org/#/Synapse:syn26009957>) and require an authorized user login. Any questions should be referred to the Lead Contact. Re-analyzed data from other available sources is listed in the Deposited Data section of Reagents and Resource. Accession numbers for all data are listed in the [key resources table](#). Microscopy data reported in this paper will be shared by the Lead Contact upon request.

All data analysis has been done by using previously published pipelines with DOIs listed in the [key resources table](#). A detailed description of the computational processing and parameters is provided in [method details](#).

Any additional information required to reanalyze the data reported in this work paper is available from the Lead Contact upon request.

EXPERIMENTAL MODEL AND SUBJECT DETAILS**Primary human samples**

Deidentified primary tissue samples were collected with previous patient consent in strict observance of the legal and institutional ethical regulations.

Protocols were approved by the Human Gamete, Embryo, and Stem Cell Research Committee (institutional review board) at the University of California, San Francisco.

Sample size estimation

Single cell RNA sequencing experiments on organoids with and without microglia were performed on three organoid cell lines, two individual organoids per condition to account for variability between different lines and organoids within the same batch. Cell counts for each individual experiment are identified in the text and figure legends.

Immunofluorescence-based imaging quantifications were performed on a minimum of three individual organoids per condition. Sample size and error bar designation are displayed in figure legends for appropriate experiments.

How subjects/samples were allocated to experimental groups

For the organoids in the presence and absence of microglia, all organoids from the experimental cohort were grown on the same plate and were randomly assigned to each experimental group.

Health/immune status

All human-derived samples came from apparently normal specimens without any known abnormalities.

Culture conditions for *in vitro* systems**Primary human microglia**

Prenatal human microglia were purified from primary human cortical brain tissue from mid-gestation (gestational week 18–23) samples using magneticactivated cell sorting kit with CD11b magnetic beads (Miltenyi Biotec, 130-049-601) following manufacturer's instructions. Briefly, primary brain tissue was minced to 1mm² pieces and enzymatically digested in 10 mL of 0.25% trypsin reconstituted from 2.5% trypsin (GIBCO, 15090046) in DPBS (GIBCO, 14190250) for 30 mins at 37°C. 0.5 mL of 10 mg/ml of DNase (Sigma Aldrich, DN25) was added in the last 5 minutes of dissociation. After the enzymatic digestion, tissue was mechanically triturated using a 10 mL pipette, filtered through a 40 µm cell strainer (Corning 352340), pelleted at 300xg for 5 minutes and washed twice with DBPS. Dissociated cells were resuspended in MACS buffer (DPBS with 1 mM EGTA and 0.5% BSA) with addition of DNase and incubated with CD11b antibody for 15 minutes on ice. After the incubation, cells were washed in a 10 mL of MACS buffer and loaded on LS columns (Miltenyi Biotec, 130-042-401) on the magnetic stand. Cells were washed 3 times with 3 mL of MACS buffer, then the column was removed from the magnetic field and microglia cells were eluted using 5 mL of MACS buffer. Cells were pelleted, re-suspended in 1 mL of culture media and counted. We routinely obtained 1x10⁶ of microglia cells per MACS purification.

Primary human microglia culture

Microglia were cultured on glass-bottom 24 well plates (Cellvis, P24-1.5H-N) pre-coated with 0.1 mg/ml of poly-d-lysine (Sigma Aldrich, P7280) for 1 hr and 1:200 laminin (Thermo Fisher, 23017015) and 1:1,000 fibronectin (Corning, 354008) for 2 hr. Microglia were plated at 1.5x10⁵ cells/well and maintained in culture media containing 66% (vol/vol) Eagle's basal medium, 25% (vol/vol) HBSS, 2% (vol/vol) B27 (Thermo Fisher, 17504001), 1% N2 supplement (Thermo Fisher, 17502001), 1% penicillin/streptomycin, and GlutaMax (Thermo Fisher, 35050061) additionally supplemented with 100 ng/ml IL34 (Peprotech, 200-34), 2 ng/ml TGFβ2 (Peprotech, 100-35B), and 1x CD lipid concentrate (Thermo Fisher, 11905031) for 5–8 days. For single cell RNA sequencing capture, cultured cells were washed with DPBS, incubated with 0.25% trypsin (Thermo Fisher, 25200056) for 10 mins at 37°C. Trypsin was inactivated by addition of DPBS with 10% FBS, the cells were centrifuged at 300x at 4°C for 5 mins and washed with DPBS twice for a total of 3 washes.

Induced microglia

Induced microglia cells were generated from human iPSC cells under defined conditions as previously described (Abud et al., 2017) and were a kind gift from Fujifilm Cellular Dynamics (iCell Microglia, 01279, catalog # RC1110).

Organoid generation

Cerebral organoids were generated based on a previously published method (Pasça et al., 2015) with several modifications. Briefly, hiPSCs cultured on Matrigel were dissociated into clumps using 0.5 mM EDTA in calcium/magnesium-free PBS and transferred into ultra-low attachment 6-well plates in neural induction media (GMEM containing 20% (v/v) KSR, 1% (v/v) penicillin-streptomycin, 1% (v/v) non-essential amino acids, 1% (v/v) sodium pyruvate, and 0.1mM 2-mercaptoethanol). For the first nine days, neural induction media was supplemented with the SMAD inhibitors SB431542 (5 µM) and dorsomorphin (2 µM), and the Wnt inhibitor IWR1-endo (3 µM), with a media exchange performed every three days. Additionally, the Rho Kinase Inhibitor Y-27632 (20 µM) was added during the first six days of neural induction to promote survival. Between days 9-25, organoids were transferred to a neural differentiation media (1:1 mixture of Neurobasal and DMEM/F12 containing 2% (v/v) B27 without vitamin A, 1% N2, 1% (v/v) non-essential amino acids, 1% (v/v) Glutamax, 1% (v/v) antibiotic/antimycotic, 0.1mM 2-mercaptoethanol) supplemented with FGFb (10 ng/mL) and EGF (10 ng/mL). Between days 25-35, organoids were maintained in neural differentiation media without FGF or EGF. From Day 35 onward, organoids were maintained in neural differentiation media containing B27 with vitamin A with media exchanges every 2-3 days.

Microglia-organoid engraftment and co-culture

Microglia from mid-gestation cortical tissue were MACS-purified and immediately added to week 5 or week 15 organoids in 6-well plates at 1×10^5 microglia cells/organoid and kept off the shaker overnight. The next day, the plates were returned to the shaker and maintained following the usual organoid maintenance protocol.

Authentication of cell lines used

All iPS cell lines used in this work has been karyotyped and regularly tested for mycoplasma. Before experiments, cortical organoids were validated for the expression of relevant brain cortex markers (Foxg1, Pax6) and presence of rosettes reminiscent of ventricular zone to confirm their cortical identity.

METHOD DETAILS

Time-lapse imaging of microglia in 2D culture

Time lapse imaging experiment for primary cultured microglia was started on day 6 of culture and continued for 24 hr in environmental control chamber (5%CO₂, 37°C and relative humidity of 70%). Imaging data were acquired using a Leica DMI-8 inverted widefield microscope, with 20x objective magnification at 0.55NA (air), and 0.4NA condensor on a Hamamatsu Flash-4 LT camera (6.5 µm pixels). The cells were held at a constant 37°C, 5% CO₂ using the Okolab stage-top incubator (H101-K-Frame). Each frame was acquired with 50 ms camera exposure. Imaging was done for a period of 24 hours at 27-minute time intervals.

Time-lapse imaging of microglia in organoids

For long-term tracking of microglia engrafted into the organoids, we achieved GFP expression with adenoviral infection. We incubated MACS-purified microglia with adenovirus CMV-GFP (E1/E5, Vector Biolabs, Cat. 1060). Briefly, freshly isolated cells were incubated with the virus for 1 hour, then washed with PBS three times to remove the viral particles, and then engrafted into organoids as previously described. Sparse GFP expression of GFP was observed after 24 hours in culture. Microglia were allowed to engraft into the organoid for seven days and then were imaged using confocal Leica SP8, 10x lens every 20 minutes for 20 hours. Image Z stacks were projected as averages. GFP-labeled microglia were used only for the imaging experiments for Figure 3A. Unlabeled microglia were used for the rest of the functional and transcriptomic evaluations.

Labeling of microglia for short-term tracking (related to Video S2) was done using CellTracker CM-Dil (Thermo Fisher, C7000). Acutely purified microglia were labeled with the cell tracker for 30 mins and then added to an organoid embedded in matrigel in a glass-bottom six-well plate (Mattek, P06G-1.5-10-F). The imaging was performed using Leica SP8 for the next 24 hours to demonstrate microglia moving toward the organoid surface and engrafting into the organoid.

Organoid single-cell capture for single-cell RNA sequencing

Two organoids per experimental condition were cut into 1 mm² pieces and enzymatically digested with papain digestion kit (Worthington, LK003163) with the addition of DNase for 1 hr at 37°C. Following enzymatic digestion, organoids were mechanically triturated using a P1000 pipette, filtered through a 40 µm cell strainer test tube (Corning 352235), pelleted at 300xg for 5 minutes and washed twice with DBPS. Cells were counted and barcoded with MULTI-seq indices (McGinnis et al., 2019) for multiplexing. Three organoid lines with and without microglia were combined and captured on two lanes of 10x Genomics using Chromium single cell 3' reagent kit (v3 Chemistry) following the manufacturer's protocol.

Single cell RNA sequencing library preparation

Single cell RNA-seq libraries were generated using the 10x Genomics Chromium 3' Gene Expression Kit. Briefly, single cells were loaded onto chromium chips with a capture target of 10,000 cells per sample. Libraries were prepared following the provided protocol and sequenced on an Illumina NovaSeq with a targeted sequencing depth of 50,000 reads per cell. BCL files from sequencing were then used as inputs to the 10X Genomics Cell Ranger pipeline.

Immunofluorescence

Cells cultured on glass-bottom well plates were fixed in 4% PFA for 10 minutes. Blocking and permeabilization were performed in a blocking solution consisting of 10% normal donkey serum, 1% Triton X-100, and 0.2% gelatin for 1 hour. Primary and secondary antibodies were diluted and incubated in the blocking solution. Cell cultures were incubated with primary antibodies at the room temperature for 1 hour, washed 3x with washing buffer (0.1% Triton X-100 in PBS), and incubated with secondary antibodies for 1 hour at the room temperature. Images were collected using Leica SP8 confocal system with 20x air objective and 63x oil objective and processed using ImageJ/Fiji and Illustrator.

Organoid samples were fixed in 4% PFA for 1 hour. Tissue sections were cryopreserved in OCT/30% sucrose (1:1) and cryosectioned at 20 μ m or 40 μ m (for synaptic density staining) thickness. Heat-induced antigen retrieval was performed in 10mM sodium citrate (pH = 6.0) for 10 min in boiling-hot solution. Blocking and permeabilization were performed in a blocking solution consisting of 10% normal donkey serum, 1% Triton X-100, and 0.2% gelatin for 1 hour. Primary and secondary antibodies were diluted and incubated in the blocking solution. Primary antibodies used in this study included: rabbit Iba1 (1:500, Wako, 019-19741) guinea pig Iba1 (1:500, Synaptic Systems, 234 004), mouse VGLUT1 (1:200, Millipore Sigma MAB5502), rabbit psd95 (1:350, Thermo Fisher, 51-6900), sheep EOMES (1:200, R&D Biosystems, AF6166), rabbit FOXG1(1:1000, Abcam, ab18259), mouse Tuj1 (1:300, Biolegend, MMS-435P), goat SOX2 (1:200, Santa Cruz Biotechnology, SC-17320), rabbit Pax6 (1:200, Biolegend, 901301), mouse Ki67 (1:200, Dako, MIB-1), rat CTIP2 (1:500, Abcam, ab18465), mouse SATB2 (1:250, Santa Cruz Biotechnology, SC-81376), mouse CD68 (1:100, Abcam, ab955), rabbit pH2AX (1:50, Cell Signaling Technologies, S139), rabbit IFITM3 (1:50, Proteintech, 11714-1-AP), rabbit P2RY12 (1:500, Sigma, HPA014518). Cryosections were incubated with primary antibodies at 4°C overnight, washed 3x with washing buffer (0.1% Triton X-100 in PBS). Secondary antibodies were species-specific AlexaFluor secondary antibodies (1:500). Images were collected using Leica SP8 confocal system with 20x air lens (0.75 NA) and 63x oil lens (1.40 NA) and processed using ImageJ/Fiji and Affinity Designer software.

Axion recordings

For MEA recordings, MACS-purified primary cortical microglia were transplanted into week 15 organoids, and the neuro-immune organoid cultures were allowed to mature for additional 5 weeks.

Multielectrode array recordings were conducted using the Axion Maestro Pro system 64 low-impedance PEDOT electrodes with 300 μ m electrode spacing. Briefly, organoids were transferred to a 64-channel multielectrode plate and equilibrated at 37°C, 5% CO₂ for at least 15 minutes prior to recording. Spontaneous neural activity was recorded for 40 mins. Firing events were defined as events with threshold amplitude of more than six standard deviations of the background noise. The event amplitude ranged between 8 μ V to over 60 μ V for some events. The majority of events consisted of multi-unit events and demonstrated waveforms characteristic for a firing neuron. The recordings at 12,500 samples/second were performed in the same media used for organoid growth. After recording, organoids were detached from the MEA plate and kept on the shaker.

QUANTIFICATION AND STATISTICAL ANALYSIS**Single cell RNA sequencing Analysis**

For preprocessing of scRNA-seq data, CellRanger was used to create a cell by gene matrix which was then processed using Cellbender (Bernstein et al., 2019) to remove ambient RNA from every run and Solo (Fleming et al., 2019) for doublet detection and removal with default parameters. A minimum of 500 unique genes, and 20% mitochondrial cutoff were used to remove low quality cells from all datasets. The data analyzed in this study were produced through the Brain Initiative Cell Census Network (BICCN: RRID:SCR_015820). To *in silico* sort microglia from all brain cells of the BICCN datasets, we selected cells expressing 10 or more cumulative UMI counts of the following genes: CCL3L3, CCL4, C3, CCL3, PLEK, FOLR2, ITGAX, SPP1, CSF3R, BIN2, DHRS9, CD74, CD69, IL1B, CX3CR1, OLR1, CH25H, FCGR2A, ADORA3, LAPT5, P2RY12, IRF8, AIF1. scRNaseq data from microglia from the developing human hippocampus (Zhong et al., 2020) was *in silico* filtered by selecting a cluster representing immune cells. After the two data sources were combined, the resulting dataset was further filtered for non-microglial cells after dimensional reduction based on preliminary clustering and marker genes that were not exhibiting canonical signatures, or other cell types. The SCTransform (Hafemeister and Satija, 2019) workflow was used and then PCA was computed on the residuals for input into Harmony (Korsunsky et al., 2019) for batch correction. The parameters of Harmony were set to use the top 20 principal components with theta set to 10. Uniform manifold approximation and projection (UMAP) (Becht et al., 2018) embeddings and neighbors for Leiden clustering (Traag et al., 2019) used the 10 components outputted from Harmony. Organoid demultiplexing and doublet filtering was done through deMULTIplex (McGinnis et al., 2019). Pearson correlation was calculated on the intersection of the shared genes between datasets which averaged Pearson residuals for each cluster. Organoid cells were batch corrected using default parameters of the SCTransform integration workflow. UCell (Andreatta and Carmona, 2021) was used to calculate gene signature scores using the top 15 genes ordered by logFC from each primary cluster calculated with a Wilcoxon rank sum test. The clusters from Leiden clustering with the highest signature score per each condition were used for joint comparison across conditions. For joint scoring of multiple conditions, all datasets were normalized using SCTransform together and the corrected normalized expression values were used for input into UCell.

Differential Expression

MAST (Finak et al., 2015) was used on log normalized raw counts was used for all differential expression tests. Wilcoxon ranked sum test was used on Pearson residuals from SCTransform for increased sensitivity on microglia treated organoids. Volcano plots were

set to have a threshold of Bonferroni corrected p value of 0.05. Differentially expressed sex genes were calculated per specific cluster using Wilcoxon rank sum test on the log normalized counts. MALAT1 and mitochondrial genes were removed from visualization but remain in the [Table S2](#).

Synapse quantification

Organoid confocal images were acquired with a Leica SP8 system. For synapse quantification, three different optical fields per organoid were imaged. For each optical field, 15 μm Z stack (0.5 μm Z-step) were collected using a 63X/1.40 oil objective. Synapse determination was based on the colocalization between Vglut1 (1:200; Millipore Sigma MAB5502) and PSD95 (1:350; Invitrogen 51-6900) as previously described ([Lehrman et al., 2018](#)) using ImageJ software. Briefly, the background was subtracted with a rolling bar radius of 10 pixels. Then, threshold was applied to every channel in order to distinguish synaptic puncta from background and generate two new binary images with the synaptic markers. Colocalization was determined overlaying both binary images with the synaptic markers. Finally, synaptic puncta were determined using the function “analyze particles.”

For volume quantification, all the volumes of synapse, lysosome and microglia are retrieved from Imaris based on the 3D-rendered structures.

IFITM3 quantification

Microglia were engrafted into week-5 organoids and were cultured as described above for seven days before being fixed. IFITM3 values were measured using ImageJ. Freehand selection tool was used to outline Sox2-positive rosettes, and then mean value intensities were measured for the three channels (DAPI, Sox2, IFITM3). IFITM3 fluorescence values were normalized to the DAPI fluorescence values to account for different number of cells in each region of interest. A two-tailed Student’s t test was used to determine significance.

pH2AX quantification

Microglia were engrafted into week-5 organoids and were cultured as described above for seven days before being fixed. pH2AX puncta were quantified using the CellProfiler 4.1.3 software ([McQuin et al., 2018](#)). The “Speckle Counting” example pipeline was modified to produce robust identification of puncta. First, Sox2+ nuclei were identified using a diameter range of 20–100 pixels, threshold strategy “Global,” and threshold method “Otsu.” The pH2AX channel was first enhanced and then masked, and puncta were subsequently counted using a diameter range of 1–10 pixels, threshold strategy “Adaptive,” and threshold method “Otsu.” A parent-child relationship was then assigned to group pH2AX puncta by Sox2+ nucleus, and the CellProfiler output was exported to Microsoft Excel. Nuclei with 0–1 or > 30 puncta were discarded, to avoid counting cells with high pH2AX signal that were actively dividing. The average number of pH2AX puncta per Sox2+ nucleus was calculated in organoid conditions with and without microglia. Then, nuclei were binned to generate a histogram of total pH2AX puncta within each bin in each condition. A two-tailed t test was used to determine significance.

Axion data analysis

Raw data from the Axion recordings were read into MATLAB then converted to numpy arrays for further processing in Python. Spikes were counted using a standard deviation threshold of 6 and converted to an array of spike times for each individual channel. Bursting activity was determined by the presence of 10 or more spikes on a given channel within one second. Next, recording time was divided into 40 ms bins and spike events were binarized based on whether or not there was at least one spike within a given time bin. Pairwise correlation between channels was determined by calculating the Pearson correlation between these binarized spike times.

ADDITIONAL RESOURCES

Figures were created using Affinity Designer software and BioRender (<https://biorender.com>).